Journal of Constructional Steel Research 197 (2022) 107489

Contents lists available at ScienceDirect

Journal of Constructional Steel Research

journal homepage: www.elsevier.com/locate/jcsr

Genetic Algorithm for the optimal placement of Self-Centering Damage-Free joints in steel MRFs

Ludovica Pieroni [a,*], Sabatino Di Benedetto [b], Fabio Freddi [a], Massimo Latour [b]

[a] Department of Civil, Environmental & Geomatic Engineering, University College of London, London, United Kingdom
[b] Department of Civil Engineering, University of Salerno, Salerno, Italy

ARTICLE INFO

Keywords:
Seismic resilience
Steel moment resisting frames
Self-centering damage-free joints
Residual drifts
Structural optimization
Genetic algorithm

ABSTRACT

Nowadays' earthquake engineering is coping with the challenging task of providing low-cost seismic resilient structures. Among others, a viable solution for seismic resilient Steel Moment Resisting Frames (MRFs) is based on the use of Self-Centering Damage-Free (SCDF) joints at Column Bases (CBs) and Beam-to-Column Joints (BCJs), ensuring both the energy dissipation capacity and self-centering behavior of the structure. Past studies demonstrated the beneficial effects gained in damage and residual drifts reduction by including SCDF joints at all BCJs and CBs. However, this solution leads to the highest structural complexity, limiting the practical application. Significant improvements can be obtained including a limited number of SCDF BCJs, but there is a lack of generalized recommendations on the number required and their effective placement. In this work, a Genetic Algorithm (GA) is proposed to define the optimal placement of SCDF BCJs in steel MRFs. The GA is implemented in Matlab, and non-linear time-history analyses are performed in OpenSees to calculate the *Fitness-Function*. The results of the GA are validated against a *Brute-Force Approach*. An 8-story 3-bays steel MRF and a type of SCDF joint are selected for case study purposes, non-linear Finite Element Models are developed in OpenSees, and the GA is applied. The results show that the proposed GA is an efficient methodology to solve the considered optimization problem.

1. Introduction

The 1994 Northridge (USA) and 1995 Kobe (Japan) earthquakes caused extensive damage to thousands of steel buildings impairing their reparability and leading, in some cases, to their demolition [1,2]. Since then, a significant effort has been made to improve the seismic design and detailing of steel constructions. Current procedures implemented in modern seismic design codes [3–5] allow meeting the life safety requirements by seismic energy dissipation based on construction damage, hence leading to significant direct (*i.e.*, casualties, repair cost) and indirect (*i.e.*, downtime) losses [6]. Furthermore, the inelastic response of the structural components can lead to significant structural permanent displacements (*i.e.*, residual deformations), which are often difficult and costly to reinstate so that the structure may be demolished, even though the collapse risk is remote [7].

Within this context, nowadays' earthquake engineering is coping with the task of providing seismic resilient steel structures able to reduce post-earthquake losses due to damage and downtime and avoid post-earthquake buildings' demolition [8–10]. As a result of the huge effort made in research, some seismic resilient technologies, such as supplemental damping devices [11–14] and base isolation systems [15–17], are nowadays implemented in international design codes and used in practice in many earthquake-prone regions [18,19]. Nevertheless, other technologies, such as self-centering systems [20–28], still require additional studies to advance the technical knowledge, enabling the transfer of academic research to policymaking and building codes. A typology of self-centering systems is based on gap opening mechanisms (*e.g.*, rocking mechanisms) controlled by elastic restoring forces usually provided by high-strength post-tensioned (PT) steel bars (or strands) and have the main advantage of preventing both structural damage and residual deformations.

For steel Moment Resisting Frames (MRFs), one viable solution is represented by the use of Self-Centering Damage-Free (SCDF) joints at Beam-to-Column Joints (BCJs) [29–31] and Column Bases (CBs) [32–34]. Most past studies [35–37] assumed the inclusion of SCDF joints in all BCJs and CBs demonstrating the beneficial effect gained in terms of reduced damage and residual deformations. However, the main challenge to the practical application of self-centering systems is related to

* Corresponding author.
E-mail address: ludovica.pieroni.20@ucl.ac.uk (L. Pieroni).

https://doi.org/10.1016/j.jcsr.2022.107489
Received 15 March 2022; Received in revised form 3 August 2022; Accepted 7 August 2022
Available online 18 August 2022

their structural complexity and cost, which could significantly exceed those of conventional solutions.

To address this issue, current research studies are investigating the use of a limited number of SCDF joints within the structure. It has been demonstrated that the exclusive use of SCDF CBs effectively reduces residual story drifts and protects the first-story columns from damage [38]. However, the results suggested that this solution is particularly effective for low-rise buildings, while its effectiveness is reduced for medium- and high-rise buildings [39]. This outcome showed that a higher number of SCDF joints is needed to obtain the desired self-centering behavior in these structures. In this context, a qualitative understanding and some preliminary recommendations for the effective placement of SCDF BCJs are provided by a recent study based on the evaluation of several *a priori*-defined configurations [40]. Nevertheless, additional studies are required in this direction. Among others, one unresolved issue is related to the development of general procedures to define the optimal placement of a limited number of SCDF BCJs in steel MRFs, which can be considered an optimization problem.

For this purpose, artificial intelligence techniques are becoming increasingly common in civil engineering thanks to the growing development of computational power in modern digital devices [41]. In particular, heuristic theories and algorithms within the framework of 'soft computing' can provide a rational and systematic way to approach and solve problems related to structural optimization [42]. Among others, Genetic Algorithms (GAs) are generation-based metaheuristic (or stochastic heuristic) algorithms initially proposed by Holland et al. [43] and built on Darwin's theory of 'evolution of species'. Due to their ability to explore the solution space and deal with mixed variables and objectives and due to their capacity to consider specific constraints, GAs are suitable for a wide variety of problems. The major advantage of GAs with respect to conventional optimization methods is that they do not require an initial estimation of the variables, and they do not differentiate the objective functions. It is worth specifying that GAs define near-optimal solutions (*i.e.*, *Most-Fit* solution), which can be different from the absolute solution (*i.e.*, *Best-Fit* solution) and, being based on random processes, they do not necessarily provide the same solution if repeatedly applied. Moreover, the choice of some key parameters is crucial in the efficacy of the GA. Therefore, it is essential to appropriately select these parameters to ensure the capability of the GA to solve the considered problem. For example, if the population size is too large, the GAs may require considerable computational effort, while if it is too small, the solution may be far from the absolute solution. However, thanks to the ability to efficiently handle discrete variables, GAs represents a good choice for structural optimization problems. A summary of the main advantages and disadvantages of GAs' method can be found in Falcone et al. [41].

One of the earliest applications of GAs in structural engineering focused on the optimization of a plane truss system [44]. Afterword, GAs have been widely used in several structural engineering optimization problems [45–52]. Specifically, several research studies have used GAs to define the optimal placement of supplemental damping devices within the structure to minimize the structural cost and maximize their efficiency. For example, Minafo' et al. [48] applied GAs to optimize the retrofitting of reinforced concrete structures investigating the optimal placement of buckling-restrained-braces. The method showed the possibility to ensure the required seismic safety level reducing intervention cost and use of materials with an optimized and structured position of the buckling-restrained braces. In another study, Wongprasert et al. [49] proposed a systematic method, based on a GA, for identifying the optimal damper distribution to control the seismic response of a 20-story benchmark building. The results demonstrated that the optimal damper locations can vary significantly depending on the considered objective function, however, most of the dampers tend to be concentrated in the lowermost and uppermost stories. Singh et al. [50] used a GA to determine the optimal size and location of viscous and viscoelastic dampers to achieve the desired performance under earthquake-induced ground motions, while Movaffaghi et al. [51] developed a GA to study the optimal placement of a given number of passive viscoelastic dampers in a steel structure in order to reduce the cost function.

In this study, a GA is developed to define the optimal placement of a given and limited number of SCDF BCJs in steel MRFs such that their effectiveness in reducing residual drifts is maximized. The proposed methodology combines artificial intelligence techniques (*i.e.,* GAs) and seismic performance assessment methods (*i.e.,* non-linear time-history analyses – NLTHAs) to solve the considered optimization problem. The procedure is based on the evaluation of several configurations with different placements of SCDF BCJs, to identify the configuration that *Most-Fit* a predefined numerical measure called *Fitness-Function*. For this purpose, a GA is implemented using a custom code written in Matlab, and NLTHAs are performed in OpenSees [53] to calculate the *Fitness-Function*. A sensitivity analysis is performed on the GA to provide the user with a qualitative understanding of how to select the GA's input parameters such that a good compromise between computational effort and accuracy of the solution is guaranteed. A *Brute-Force Approach*, investigating all the possible configurations with different placements of the SCDF BCJs, is carried out, and the results are used to validate the effectiveness and efficiency of the GA. An 8-story 3-bays steel MRF is selected as a case study structure, and a type of SCDF joint is taken into account [33]. A detailed description of the methodology used in the study is reported in the following Section.

2. Methodology

The optimization problem considered in this study aims at defining the optimal placement of a given and limited number of SCDF BCJs (n_{BCJ}) within steel MRFs. The following assumptions are considered for the placement: *i)* the inclusion of SCDF CBs in all configurations, *ii)* the symmetric placement of SCDF BCJs, *iii)* the inclusion of the same number of internal ($n_{BCJ\text{-}INT}$) and external ($n_{BCJ\text{-}EXT}$) SCDF BCJs. Moreover, to examine an additional aspect of the optimization problem, the *Story-Restraint* condition is defined and used at different steps of the study. The *Story-Restraint* consists of assuming that all the BCJs belonging to the same story are characterized by the same properties (*i.e.,* all conventional or all SCDF BCJs). The *Story-Restraint* is considered an option to reduce the number of possible configurations with different placements of the limited number of SCDF BCJs.

Fig. 1 shows the methodology used to solve the optimization problem which includes three steps (A, B, and C).

Step A describes the properties, design, and modeling of the considered case study structure. In particular, an 8-story 3-bays steel MRF is selected for case study purposes, and the system proposed and experimentally investigated by Latour et al. [33] is considered as SCDF joint. Although a specific typology of SCDF joint is assumed, the proposed methodology can be applied to any other SCDF system showing a similar moment-rotation behavior (*i.e.*, flag-shape behavior). Two reference configurations are considered: the MRF with conventional CBs and full-strength BCJs (indicated as MRF), and the equivalent MRF with all SCDF CBs and BCJs (indicated as M-BCJ). Moreover, four scenarios are defined based on a given and limited number of SCDF BCJs (n_{BCJ}) to be included in the case study steel MRF (indicated as S4, S8, S12, S16). The conventional MRF is designed according to Eurocode 8 [4] requirements, while the SCDF joints are designed following a tailored design procedure previously proposed by the Authors [40]. Non-linear Finite Elements (FE) models are developed in OpenSees [53]. Further details are provided in Section 3; specifically, Subsection 3.1 describes the properties of the steel MRF and the SCDF joint, 3.2 describes the properties of the investigated scenarios, 3.3 illustrates the design procedure, and 3.4 presents the FE model.

Step B describes the GA developed to solve the considered optimization problem and is divided into three parts: *1)* implementation, *2)* sensitivity analysis, and *3)* validation. The GA is implemented using a custom code written in Matlab where the *Fitness-Function* is based on the

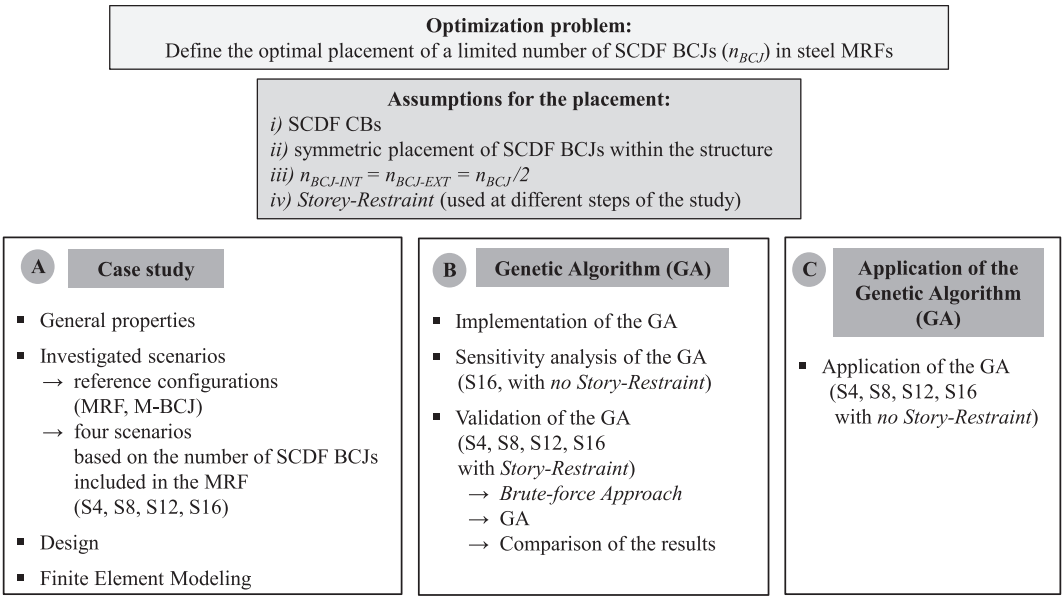

Fig. 1. Methodology: Optimal placement of a limited number of Self-Centering Damage-Free Beam-to-Column Joints (SCDF BCJs) in steel Moment Resisting Frames (MRFs) through Genetic Algorithm (GA).

residual interstory drifts determined by performing NLTHAs in OpenSees [53]. A sensitivity analysis is performed on the GA to provide a qualitative understanding of how to choose the input parameters. Successively, the GA is validated by comparison with the results of a *Brute-Force Approach*. Further details are provided in Section 4; specifically, Subsection 4.1 describes the implementation, 4.3 the sensitivity analysis, and 4.4 the validation.

Step C describes the application of the GA to all the scenarios with *no Story-Restraint*. It is demonstrated that the GA defines a solution for the optimization problem by investigating a limited and small percentage of the possible configurations with different placements of the SCDF BCJs. Further details are provided in Section 5, which presents and critically discusses the application of the GA to the investigated scenarios.

3. Case study and finite element model

3.1. Description of the case study structure

The following Subsections contain a synthetic description of the selected case study structure with the essential information. Additional details can be found in Pieroni et al. [40].

Fig. 2 (a) and (b) illustrate respectively the plan and elevation views of the 8-story, 3-bay steel MRF selected as case study structure. The current study focuses on one of the two perimeter MRFs in the *x*-direction.

The SCDF joint proposed and experimentally investigated by Latour et al. [33] is considered. Fig. 3 shows the SCDF joint adopted for CBs and BCJs in their deformed shape, *i.e.,* rocking mechanism. The SCDF joint consists of: *i)* a system of FDs composed of steel plates with slotted holes and friction pads fastened together by pre-loaded bolts to dissipate the seismic input energy through the alternate slippage of the surfaces in contact, *ii)* a system of PT bars and disk springs to control the self-centering behavior. Disk springs are placed in series and parallel to control the stiffness and resistance of the self-centering system. Fig. 3 also shows the forces in the SCDF joints during the rocking mechanism, including the force in the web-FD (F_w), the force in the flanges-FDs (F_f), the force in the PT bars (F_{PT}), the compression force (F_c) at the center of rotation (COR). It is worth clarifying that external and internal SCDF BCJs are slightly different. Fig. 3 (a) and (b) represent respectively a SCDF CB and an external SCDF BCJ. In the internal SCDF BCJs the PT bars cross the joint uninterruptedly from one side to the other, and the rocking mechanism happens at both sides of the beam-to-column intersection.

Fig. 4 shows the moment-rotation behavior of the SCDF joint (*i.e.*,

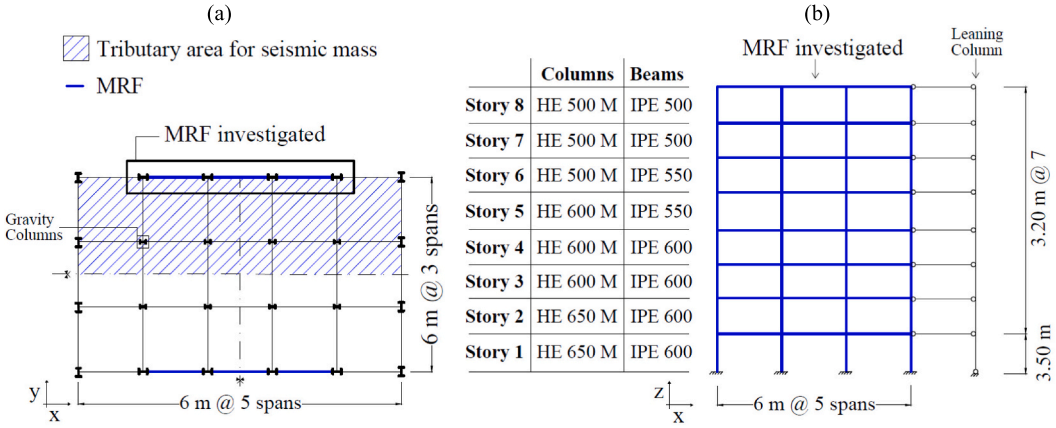

	Columns	Beams
Story 8	HE 500 M	IPE 500
Story 7	HE 500 M	IPE 500
Story 6	HE 500 M	IPE 550
Story 5	HE 600 M	IPE 550
Story 4	HE 600 M	IPE 600
Story 3	HE 600 M	IPE 600
Story 2	HE 650 M	IPE 600
Story 1	HE 650 M	IPE 600

Fig. 2. Case study structure. (a) Plan view. (b) Elevation view with columns' and beams' cross-sections (Adapted from Pieroni et al. [40]).

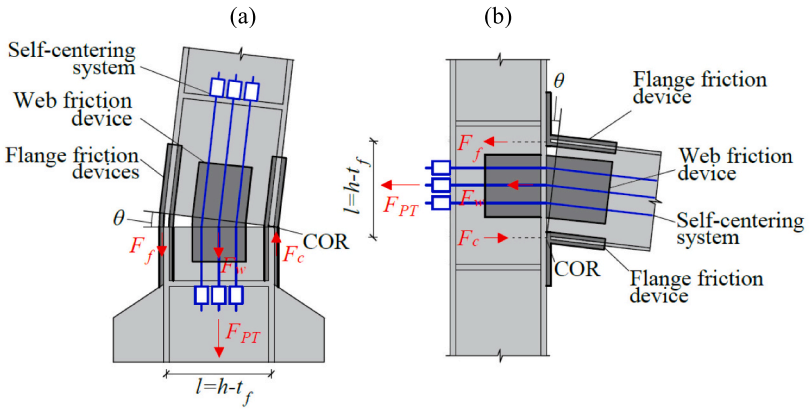

Fig. 3. Self-Centering Damage-Free (SCDF) Joints for: (a) Column Bases (SCDF CBs); (b) External Beam-to-Column Joints (SCDF BCJs) (Adapted from Pieroni et al. [40]).

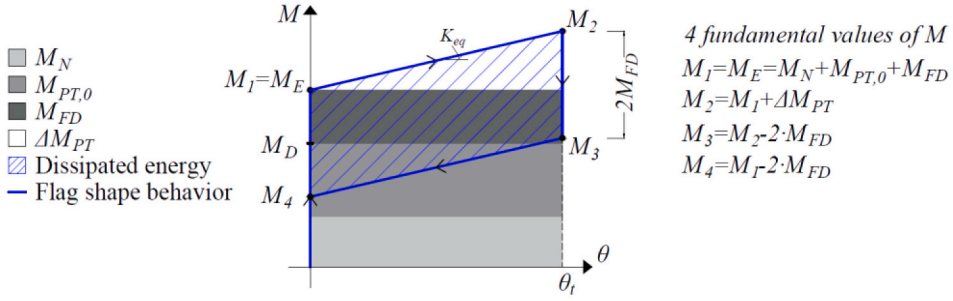

Fig. 4. Moment-rotation behavior of the Self-Centering Damage-Free joints (Adapted from Pieroni et al. [40]).

flag-shape hysteretic behavior) and the four fundamental values of the moment, *i.e.*, the max and min moment at zero (M_1, M_4) and at target rotation θ_t (M_2, M_3). In the present study, the target rotation of the joint (θ_t) is assumed equal to 40 mrad, which is the benchmark rotation established by AISC 341–16 [3] for Special MRFs. The interested reader is referred to Latour et al. and Elettore et al. [33,38] for further details about the structural configuration of the SCDF joint, the expected forces in the components, and the moment-rotation behavior.

3.2. Investigated scenarios

Two reference configurations are considered: the MRF with conventional CBs and full-strength BCJs (indicated as MRF), and the equivalent MRF with all SCDF CBs and BCJs (indicated as M-BCJ). Past studies [40] demonstrated that these two configurations do not represent optimal solutions. From one side, conventional steel MRFs experience large residual drifts; on the other side, including SCDF joints in all CBs and BCJs ensures a self-centering behavior but leads to the highest cost and structural complexity.

Within this context, this study aims to solve the optimization problem by considering SCDF CBs and a limited number of SCDF BCJs (n_{BCJ}) to be implemented in the structure such that their effectiveness is maximized, and their structural complexity and cost are minimized. Four scenarios are defined based on the number of SCDF BCJs (n_{BCJ}): S4, S8, S12, and S16, characterized respectively by n_{BCJ} equal to 4, 8, 12, and 16. It is worth recalling that the considered case study structure has 32 BCJs (*i.e.*, 16 external BCJs and 16 internal BCJs). Moreover, according to the assumptions considered for the placement (Section 2), the same number of internal ($n_{BCJ\text{-}INT}$) and external ($n_{BCJ\text{-}EXT}$) SCDF BCJs are included in the MRF. Table 1 reports the main properties of each scenario in terms of the number of SCDF BCJs to be included in the structure (*i.e.*, n_{BCJ}, $n_{BCJ\text{-}INT}$, $n_{BCJ\text{-}EXT}$).

Table 1
Properties of the four investigated scenarios (*i.e.*, S4, S8, S12, S16): number of total (n_{BCJ}), internal ($n_{BCJ\text{-}INT} = n_{BCJ}/2$), external ($n_{BCJ\text{-}EXT} = n_{BCJ}/2$) Self-Centering Damage-Free Beam-to-Column Joints (SCDF BCJs) to be included.

S	n_{BCJ}	$n_{BCJ\text{-}INT}$	$n_{BCJ\text{-}EXT}$
S4	4	2	2
S8	8	4	4
S12	12	6	6
S16	16	8	8

3.3. Design of the case study structure

The conventional MRF (*i.e.*, the reference configuration with conventional CBs and full-strength BCJs – indicated as MRF) is designed according to Eurocode 8 [4], considering steel grade S355 for columns and S275 for the beams, and plan and elevation regularity. The design earthquake at the Ultimate Limit State (ULS [4] – probability of exceedance of 10% in 50 years) is defined considering Type 1 elastic response spectrum with a peak ground acceleration of 0.35 g, soil type C, and an importance class II (*i.e.,* ordinary buildings). The behavior factor (q) is assumed equal to 6.5, according to the provisions of Eurocode 8 [4] for MRFs in high ductility class. The non-structural elements are assumed 'fixed in a way so as not to interfere with structural deformations'; therefore, the interstory drift limit for the Damage Limit State (DLS [4] – probability of exceedance of 10% in 10 years) is assumed as 1%, accordingly with the Eurocode 8 [4]. Fig. 2 (b) shows beams' and columns' profiles obtained from the design.

The self-centering MRFs (*i.e.*, the reference configuration with all SCDF CBs and BCJs – indicated as M-BCJs – and all the configurations with different placements of SCDF BCJs investigated in each scenario – indicated as S4, S8, S12, S16) are obtained by including SCDF CBs and BCJs at specific locations within the conventional MRF. The SCDF CBs

and BCJs are designed following a tailored design procedure proposed by Pieroni et al. [40], which takes into account the random variability related to the properties of the joint's elements (*i.e.*, the friction coefficient of the FDs, the post-tensioning forces in the PT bars). The design's objectives are: *i)* no yielding of the structural element (*i.e.*, $M_2 < M_y$), *ii)* self-centering behavior of the structure (*i.e.*, $M_4 < 0$), *iii)* bending moment at the gap opening higher than the one under the ULS seismic combination of Eurocode 8 [4] (*i.e.*, $M_1 > M_{Ed}$). The design procedure is applied for SCDF CBs and BCJs.

Fig. 5 (a) shows a schematic representation of the locations of the different moment-rotation behaviors designed for SCDF CBs and BCJs.

For SCDF BCJs three different types of moment-rotation behavior are defined based on the beams' cross-section as represented in Fig. 5 (a). Fig. 5 (b) shows the three moment-rotation behaviors and the corresponding beam's yielding moments (M_y). The maximum moment of the moment-rotation behavior (M_2) is reduced while reducing the dimension of the beams' sections, thus the yielding moment. *t1–4*, *t5–6*, and *t7–8* are characterized by a similar self-centering capacity, while the dissipative capacity significantly decreases from *t1–4* to *t7–8*.

For SCDF CBs two different types of moment-rotation behavior are defined for external and internal CBs. Fig. 5 (a) and (b) show the moment-rotation behavior obtained respectively for the external and internal SCDF CBs. In both figures, the dashed black lines represent the yielding moment of the column cross-section (M_y) strengthened with steel plates welded to the flanges, while the dot-dashed corresponds to the bending moment occurring in the column under the ULS seismic combination of Eurocode 8 [4] (M_{Ed}). It is worth mentioning that during the seismic event the external columns (Fig. 5 (a)) are subjected to high variability of the axial force (*i.e.*, $N_{Ed,min}$ *[tension]* << $N_{Ed,max}$ *[compression]*), while internal columns (Fig. 5 (b)) are subjected to very similar values of compression (*i.e.*, $N_{Ed,min} \sim N_{Ed,max}$).

3.4. Finite element modeling

Two-dimensional non-linear FE models are developed in OpenSees [53] for the MRF and self-centering MRFs. The 'Steel01' material [53] with 275 and 355 MPa yield strength is used for beams and columns, respectively, and a 0.2% post yield stiffness ratio is used in both cases. Columns are modeled as non-linear elements with distributed plasticity ('nonlinearBeamColumn element' [53]), and the 'Scissor' model [54] is used for the panel zones. Beams are modeled based on a lumped plasticity approach. Specifically, for the conventional MRF, zero-length non-linear rotational springs ('zeroLength element' [53]) are placed at beams' ends to simulate the formation of plastic hinges. The rotational springs are defined with a bilinear hysteretic moment-rotation behavior ('uniaxialMaterial Bilin' [53]) based on the modified Ibarra–Krawinkler deterioration model [55] implemented as suggested by Lignos and Krawinkler [56]. Contrary, for the self-centering MRFs, the beams' ends and the CBs are implemented with SCDF joints. Fig. 6 (a) shows a schematic representation of the advanced modeling strategy adopted for SCDF CBs previously used by the Authors [38,39,57]. It consists of a sophisticated two-dimensional non-linear FE model where each component is modeled independently and has the main advantage of taking into account the variability of the axial force in columns during the seismic event. Conversely, Fig. 6 (b) shows a schematic representation of the simplified modeling strategy adopted for SCDF BCJs implemented following a simplified modeling strategy used in Pieroni et al. [40]. It consists of a non-linear rotational spring allocated at beams' ends and characterized by the flag-shape moment-rotation behavior of the SCDF joint. Further details on the FE models of the conventional MRF and self-centering MRFs can be found in Pieroni et al. [40].

It is worth reminding the reader that in the M-BCJ (*i.e.*, the reference configuration with all SCDF CBs and BCJs) all BCJs are modeled with the SCDF strategy. Conversely, in the other self-centering MRFs (*i.e.*, the configurations with different placements of SCDF BCJs investigated in

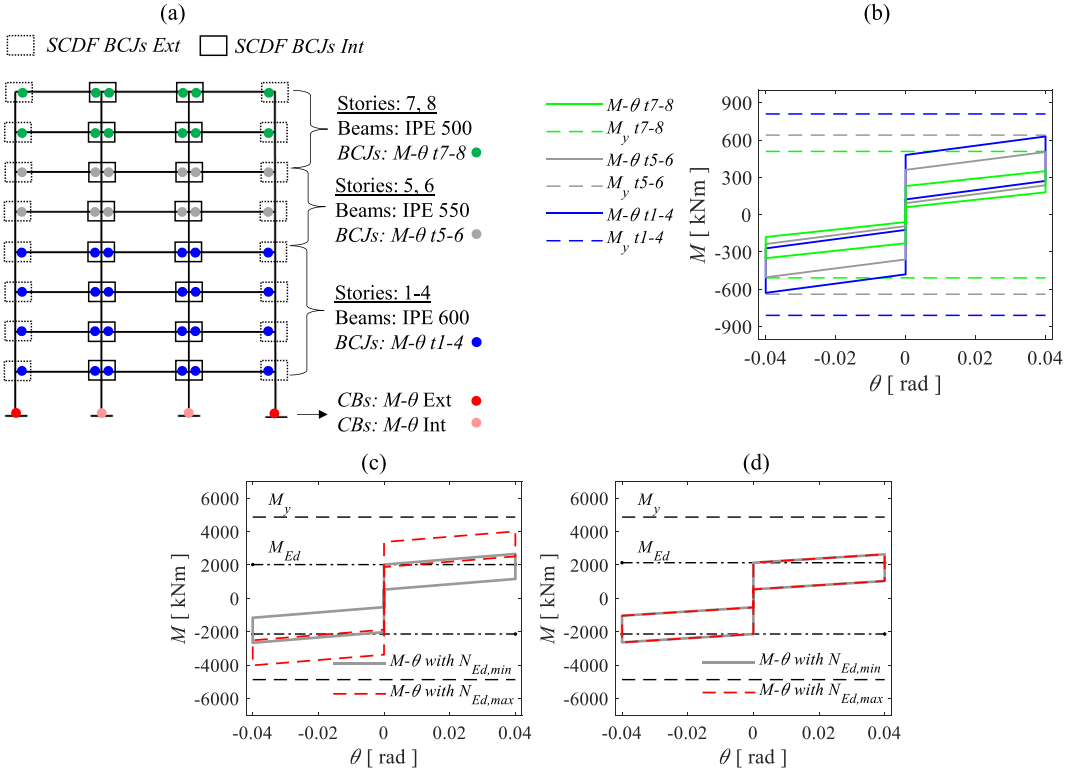

Fig. 5. Design of the Self-Centering Damage-Free Column Bases (SCDF CBs) and Beam-to-Column Joints (SCDF BCJs). (a) Location of the joints. Moment-rotation behaviors of: (b) SCDF BCJs at stories 1–4, 5,6 and 7,8 (*i.e., t1–4, t5–6, t7–8*), (c) external SCDF CBs, (d) internal SCDF CBs (Adapted from Pieroni et al. [40]).

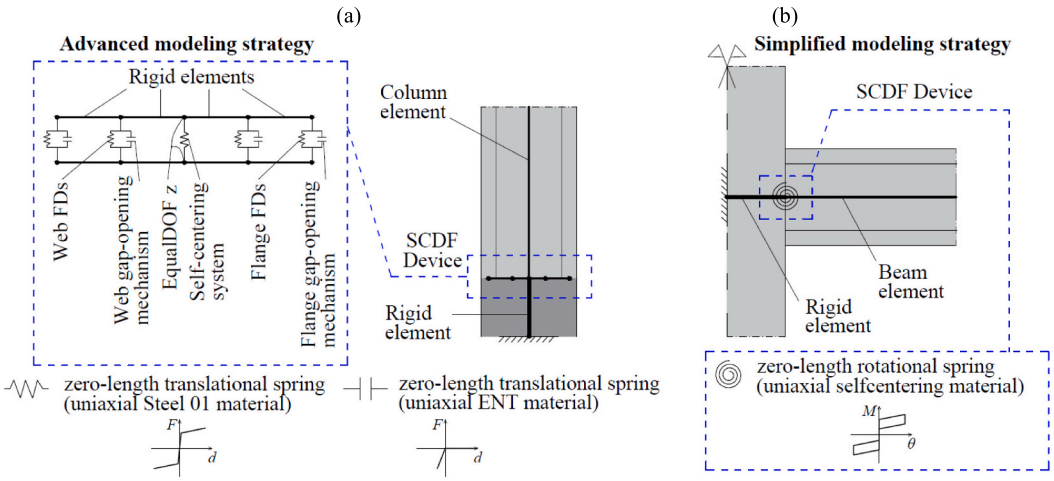

Fig. 6. Finite Element Modeling of the Self-Centering Damage-Free (SCDF) joints. (a) Advanced modeling strategy for SCDF CBs. (b) Simplified modeling strategy for SCDF BCJs (Adapted from Pieroni et al. [40]).

each scenario), the BCJs are implemented with the conventional or SCDF strategy based on the placements of the SCDF joints.

4. Genetic Algorithm (GA)

Genetic Algorithms (GAs) are random processes that simulate Darwin's evolutionary theory of individuals based on a selection principle that follows the 'survival of the strongest' rule. The search for the solution begins with an initial generation of individuals who are evaluated relative to a given measure of fitness (*i.e.*, the *Fitness-Function*). The *Most-Fit* individuals are selected, and they give rise to the next generation using operations such as *Random Mutation* and *Cross-Over*. The basic components of all GAs are the following:

i) An initial generation of individuals. The individuals are the candidate solutions that the GA seeks and evaluates at each generation. Generations are often represented by matrixes where columns represent the individuals.
ii) *Random Mutation* and *Cross-Over* operators. *Random Mutation* and *Cross-Over* are the two operators used to create new individuals in the new generations. They are both based on the *Most-Fit* individuals of previous generations (*i.e.*, *Parent-Individuals*). The *Random Mutation* produces random changes to some chosen individuals to create new individuals. The *Cross-Over* swaps a subsequence of two chosen individuals to create new individuals.
iii) A *Fitness-Function*. The *Fitness-Function* is the function that the GA tries to optimize. It is one of the most decisive parts of the GA, and it is used to quantify how *Fit* each individual is.
iv) A selection criterium for which individuals will reproduce. The selection operator selects the *Most-Fit* individuals to be used as *Parent-Individuals* to generate new individuals in the new generations. It is based on the *Fitness-Function*, and it is thought such that the fitter an individual is, the more likely it is to be selected.

In the present study, a GA is developed to define the optimal placement of a given and limited number of SCDF BCJs (n_{BCJ}) in steel MRFs. Within this context, the individuals represent the configurations with different placements of the SCDF BCJs, and the *Fitness-Function* represents the effectiveness of the placement in terms of self-centering capability.

This Section is divided into three Subsections; specifically, Subsection 4.1 describes the implementation and hence the steps and properties of the developed GA, 4.3 presents a sensitivity analysis performed on the GA, and 4.4, presents the validation of the GA by comparison with the results obtained from the *Brute-Force Approach*.

4.1. Description of the Genetic Algorithm (GA)

Fig. 7 shows a schematic representation of the six main steps of the GA developed in this study.

The developed GA requires the following input parameters: the number of internal and external SCDF BCJs to be included in the structure ($n_{BCJ\text{-}INT,}$ $n_{BCJ\text{-}EXT}$), the number of generations (G) to be analyzed, the number of new individuals generated by random mutation in each generation (I).

The individuals represent the configurations with different placements of the SCDF BCJs. Thanks to the symmetric placement of the SCDF joints within the structure, the implementation of the GA can be simplified by considering only half of the structure (*i.e.*, 16 BCJs instead of 32 BCJs). Therefore, the number of internal and external SCDF BCJs used in the GA refer to half structure (*i.e.*, $n_{BCJ\text{-}INT\text{-}h} = n_{BCJ\text{-}INT}/2$, $n_{BCJ\text{-}EXT\text{-}h=} = n_{BCJ\text{-}EXT}/2$). The individuals are implemented by column vectors with 16 rows where each element represent a specific position. Particularly, rows 1 to 8 refer to external BCJs from story 1 (*i.e.,* row 1) to story 8 (*i.e.,* row 8), and rows 9 to 16 refer to internal BCJs from story 1 (*i.e.,* row 9) to story 8 (*i.e.,* row 16). Vectors are composed of decimal numbers between 0 and 1. The generations are represented by matrixes where each column represents a single individual with 16 rows. It is worth mentioning that when the *Story-Restraint* is used, the GA can be further simplified. The *Story-Restraint* assumes that in each story, external and internal BCJs have the same properties (*i.e.,* all conventional BCJs or all SCDF BCJs); therefore, it is possible to consider only the external BCJs in half of the structure (*i.e.,* 8 BCJs instead 32 BCJs) and assuming that the internal BCJs and the other half part of the structure have the same properties.

Step 1 of the GA consists of two independent operators (*i.e., Random Mutation* and *Cross-Over*), which create new individuals for every new generation based on *Parent-Individuals*. The new individuals generated in this step are then merged in Step 2 of the GA. The *Random Mutation* generates a number of new individuals (I) based on a *Parent-Individual* (i_{p1}). For generation 1, i_{p1} is an initial random individual, while for the following generations, i_{p1} *is* the *Most-Fit* individual selected from the previous generations (see Step 6 of the GA). In the *Random Mutation*, the elements of i_{p1} are altered by adding random quantities between −0.5 and 0.5 (*i.e.,* variation 1) to create new individuals, referred as $i_{mi\ (i=1:I)}$. Successively, the elements of the new individuals are rounded into Boolean values (*i.e.,* 0 or 1), where 0 stands for 'conventional BCJ' and 1 stands for 'self-centering BCJ'. It is worth specifying that if negative numbers occur, they are rounded to 0, while numbers exceeding 1 are rounded to 1. Assuming a random variation of the initial element equal to 1 (*i.e.,* ± 0.5), each element of i_{p1} (*i.e.,* each specific position)

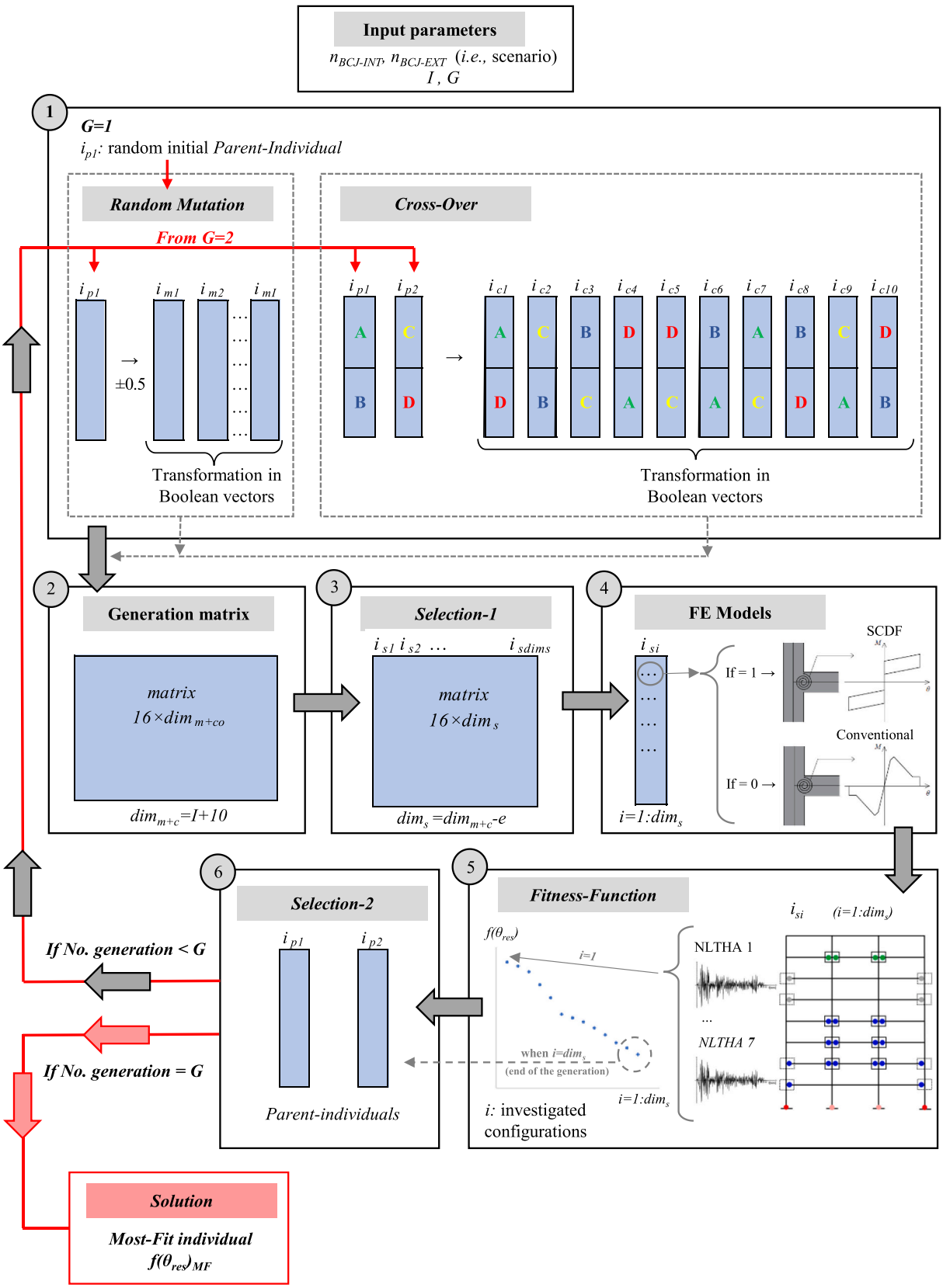

Fig. 7. Main steps of the Genetic Algorithm (GA).

potentially has the chance to change from 0 (*i.e.,* absence of SCDF joint) to 1 (*i.e.*, presence of SCDF joint) and vice-versa. The *Cross-Over* is performed from generation 2 and generates 10 new individuals based on two *Parent-Individuals* (i_{p1} and i_{p2}) selected from the previous generations as the two *Most-Fit* individuals (see Step 6). This operation (*i.e.,* single-point *Cross-Over*) consists in splitting i_{p1} and i_{p2} (*i.e.,* 16×1 column vectors) into two strings (*i.e.,* 2 strings of 8×1 column vectors) and shuffling them to create 10 new individuals. Successively, the elements of the new individuals are rounded into Boolean values (*i.e.,* 0 or 1) as discussed for the *Random Mutation*. The new individuals generated by the *Cross-Over* are referred as $i_{ci\ (i=1:10)}$. A graphical representation of *Cross-Over* is shown in Fig. 7.

Step 2 of the GA merges the new individuals generated independently from the *Random Mutation* (i_m) and the *Cross-Over* (i_c) to create a ($16 \times dim_{m+c}$) generation matrix.

Step 3 of the GA applies the *Selection-1* operator. The *Selection-1* is applied after the *Random Mutation* and *Cross-Over* when the individuals are represented by Boolean vectors of 0s and 1s. It has two main objectives: *i)* selecting the individuals with a number of internal and external SCDF BCJs equal to the assumed input parameters (*i.e.,* the sum of 1s from rows 1 to 8 is equal to $n_{BCJ\text{-}INT\text{-}h}$, and the sum of 1s from rows 9 to 16 is equal to $n_{BCJ\text{-}EXT\text{-}h}$), *ii)* selecting the unique individuals by removing the individuals which are repeated in the current generation or already investigated in the previous generations. The criteria of the *Selection-1* operator can be summarized as follows:

$$Selection-1 \rightarrow \begin{cases} \left(\sum_{r_i=1}^{8} i(r_i)\right) = n_{BCJ-EXT\_h} \\ \left(\sum_{r_e=9}^{16} i(r_e)\right) = n_{BCJ-INT\_h} \\ no\ duplicates\ (in\ the\ current\ and\ previous\ generations) \end{cases} \quad (1)$$

where r_i *and* r_e are the number of rows representing respectively the internal and external joints, i are the individuals in the generation matrix, $n_{BCJ\text{-}EXT\text{-}h}$ and $n_{BCJ\text{-}INT\text{-}h}$ are the number of internal and external SCDF BCJs to be included in half structure. Therefore after *Selection-1*, the generation matrix is a $16 \times dim_s$ matrix and contains the selected individuals, which are referred as $i_{si\ (i=1:dims)}$.

It is worth highlighting that the second dimension of the generation matrix (*i.e.,* number of columns) varies during the GA. It is equal to dim_{m+c} after *Random Mutation* and *Cross-Over* and dim_s after the *Selection-1*. They can be calculated as follows:

$$dim_{m+c} = I + 10; dim_s = dim_{m+c} - e \quad (2)$$

where I and *10* are the numbers of new individuals generated respectively by the *Random Mutation* and *Cross-Over*, while e is the number of individuals removed by the *Selection-1* operator.

It's important to clarify that dim_s corresponds to the number of individuals investigated in a generation. Therefore, the total number of individuals (*i.e.,* configurations with different placements of the SCDF BCJs) investigated in the GA (C_{GA}) can be calculated as follows:

$$C_{GA} = \sum_{i=1}^{G} dim_s \quad (3)$$

where G is the number of analyzed generations and dim_s is the number of individuals after *Selection-1* in each generation.

Step 4 of the GA creates the FE models in OpenSees [53]. For each individual selected in Step 3 of the GA (i_s), a non-linear FE model is developed in OpenSees [53], including SCDF CBs and SCDF BCJs at specific locations according to the information contained in the individuals' vector.

Step 5 of the GA consists of evaluating the selected individuals through the *Fitness-Function*. The *Fitness-Function* is defined as the median value of the residual interstory drifts (θ_{res}) obtained at each story performing seven NLTHAs, hence accounting for the influence of the uncertainty related to the earthquake input (*i.e.,* record-to-record variability). For each individual, seven NLTHAs are performed on the corresponding FE model developed in Step 4 of the GA, story-level Engineering Demand Parameters, such as residual interstory drifts (θ_{res}), are monitored, and the *Fitness-Function* ($f(\theta_{res})$) is calculated as follows:

$$f(\theta_{res}) = median\left[(\theta_{res})_{1:s}\right]_{1:GM} \quad (4)$$

where s is the number of stories, and GM is the number of NLTHAs (*i.e.,* 7 ground motions records in the present study, see Subsection 4.2). According to this definition, in the present study, the smaller the *Fitness-Function* $f(\theta_{res})$ is (*i.e.,* smaller residual interstory drifts), the more fit an individual is (*i.e.,* more effective placement of the SCDF BCJS).

Step 6 of the GA consists of the application of the *Selection-2* operator. This operator selects, among the individuals investigated in the current and previous generations, the two *Most-Fit* individuals (*i.e.,* with the smaller values of $f(\theta_{res})$). These two individuals are referred to as *Parent-Individuals* (i_{p1} and i_{p2}) and are used in the next generation by the *Random Mutation* and the *Cross-Over* to generate a new matrix of new individuals (Step 1 of the GA).

The just described Steps are repeated for each generation, and the GA stops when a number of generations equal to G are analyzed. The solution of the GA is represented by the *Most-Fit* individual among all the investigated individuals, and its *Fitness-Function* is referred to as $f(\theta_{res})_{MF.}$ Therefore, given a limited number of SCDF BCJs (n_{BCJ}) to be included in the structure, the solution of the GA is the configuration with the optimal placement of the SCDF BCJs, which minimizes the residual interstory drifts maximizing the self-centering capability of the structure.

4.2. Ground motion records

A set of 7 ground motion records is selected from the SIMBAD Database using REXEL [58] to perform the NLTHAs in Step 5 of the GA (Fig. 7). The configurations are characterized by slightly different values of the fundamental vibration period due to the different stiffness of the joints. Therefore, the mean fundamental period among all configurations ($T_{1m} = 1.27$ s) is considered. The following input parameters are used for the selection: moment magnitude (M_w) ranging from 6 to 7, epicentral distance $R \leq 30$ *km*, and spectrum compatibility in the range of periods between $0.2T_{1m}$ and $2T_{1m}$, where $T_{1m} = 1.27$ s represents the mean fundamental period among all configurations. The mean elastic spectrum of the records is kept between 75% and 130% of the corresponding Eurocode 8 [4] elastic response spectrum considered for the design. The results of the ground motion selection are shown in Fig. 8 (a). A large number of zero acceleration points (*i.e.,* 40 s) have been added at the end of each record to allow the free vibrations to stop and correctly capture the residual deformations. The spectral acceleration (S_a) at T_{1m} is considered as Intensity Measure (IM). The selected ground motion records are scaled to an IM equal to 0.6 g, corresponding to the ULS seismic intensity (Fig. 8 (b)), and applied to the different configurations performing NLTHAs.

4.3. Input parameters and sensitivity analysis of the Genetic Algorithm (GA)

Some input parameters of the GA are chosen by the user and need careful consideration. The number of internal and external SCDF BCJs to be included in the structure ($n_{BCJ\text{-}INT}$, $n_{BCJ\text{-}EXT}$) are chosen based on the investigated scenario and are a function of the geometry of the structure. Conversely, the number of generations (G) to be analyzed and the number of new individuals generated by *Random Mutation* in each generation (I) need further discussion since they significantly affect the number of investigated configurations (C_{GA}) and the solution (*Most-Fit*

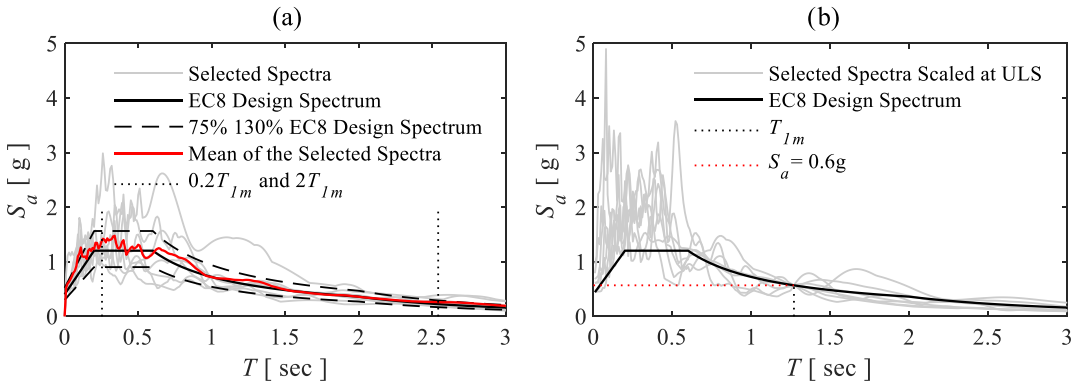

Fig. 8. (a) Ground motions selection. (b) Ground motions records scaled at a spectral acceleretion corresponding to the Ultimate Lilim State (*i.e.*, $S_a(T_{1m}) = 0.6$ g).

individual with $f(\theta_{res})_{MF}$) of the GA.

Due to its dependence on *G* and *I* and its randomness, the GA cannot ensure that the obtained *Most-Fit* individual is the *Best-Fit* individual (*i.e.*, $f(\theta_{res})_{MF}$ can be different from $f(\theta_{res})_{BF}$) and provide the same solution if repeatedly applied (*i.e.,* different values of $f(\theta_{res})_{MF}$). Choosing large values of *G* and *I* such that a large number of individuals are evaluated, on one side is convenient because it allows for a higher likelihood of finding a *Most-Fit* individual who is close or equal to the *Best-Fit* individual (*i.e.*, $f(\theta_{res})_{MF} \sim f(\theta_{res})_{BF}$), but on the other side it leads to a higher computational effort. Therefore, the values of *G* and *I* need to be appropriately selected.

Within this context, a sensitivity analysis is performed on the GA with the following objectives: *i)* analyze the effects of the input parameters *G* and *I*, *ii)* evaluate the effect of the intrinsic randomness, *iii)* provide the user with a qualitative understanding on how to select the input parameters *G* and *I*.

Scenario S16 with *no Story-Restraint* is used for the sensitivity analysis. Given a limited number of SCDF BCJs (n_{BCJ}) to be included in the MRF with *no Story-Restraint*, the number of possible individuals (C_P), *i.e.*, configurations with different placements, can be calculated using the following equation (*i.e.*, the product of the combinations of permutations without repetition for internal and external BCJs):

$$C_P = \left(\frac{n!}{r!(n-r)!}\right)_{EXT} \cdot \left(\frac{n!}{r!(n-r)!}\right)_{INT} \tag{5}$$

where *n* is the number of internal or external BCJs in half structure (*i.e.*, 8) and *r* is the number of internal or external SCDF BCJs to be included in half structure (*i.e.*, $n_{BCJ\text{-}INT\_h}$, $n_{BCJ\text{-}EXT\_h}$). For S16, $n_{BCJ\text{-}INT\_h}$ and $n_{BCJ\text{-}EXT\_h}$ are equal to 4 (*i.e.*, $n = 8$, $r = 4$), therefore the number of possible individuals (C_P) is 4900.

Different values of *G* and *I* are considered, and for each (*G, I*) couple, the GA (Subsection 4.1) is repeated 10 times (*i.e.,* 10 simulations) to account for its randomness. Two sets of values are selected for both *G* and *I (i.e.*, 5, 10, 15, 20 and 25, 50, 75, 100*)*, and then combined into thirty-two different couples of (*G, I*) reported in Table 2. It is worth highlighting that this part of the study required a total of 271,887 NLTHAs. To provide a more detailed understanding of the sensitivity analysis, the results are firstly shown for two values of *G* (*i.e.*, 15 and 75), and successively considerations on the whole sets of results are made.

Fig. 9 shows the results obtained for *G* equal to 15, and *I* equal to 5, 10, 15, and 20, and for *G* equal to 75, and *I* equal to 25, 50, 75, and 100. Each descendent trend refers to one of the 10 simulations of a specific (*G, I*). The values of the *Fitness-Function* ($f(\theta_{res})$) for all the investigated individuals are reported on the *y*-axis, while the *x*-axis shows the progressive number of investigated individuals. The bigger dots represent the solution of the GA, hence the *Most-Fit* individual ($f(\theta_{res})_{MF}$) and the total number of investigated individuals (C_{GA}). The descendent trends obtained in each simulation show how the GA is able to create progressively more fit individuals characterized by smaller values of $f(\theta_{res})$.

Table 2
Couples of (*G, I*) investigated in the sensitivity analysis.

Values of *G*	Values of *I*	Investigated couples (*G, I*)			
5	5, 10, 15, 20	(*G5, I5*)	(*G5, I10*)	(*G5, I15*)	(*G5, I20*)
10		(*G10, I5*)	(*G10, I10*)	(*G10, I15*)	(*G10, I20*)
15		**(*G15, I5*)**	**(*G15, I10*)**	**(*G15, I15*)**	**(*G15, I20*)**
20		(*G20, I5*)	(*G20, I10*)	(*G20, I15*)	(*G20, I20*)
25	25, 50, 75, 100	(*G25, I25*)	(*G25, I50*)	(*G25, I75*)	(*G25, I100*)
50		(*G50, I25*)	(*G50, I50*)	(*G50, I75*)	(*G50, I100*)
75		**(*G75, I25*)**	**(*G75, I50*)**	**(*G75, I75*)**	**(*G75, I100*)**
100		(*G100, I25*)	(*G100, I50*)	(*G100, I75*)	(*G100, I100*)

Note: The bold characters represent the (*G, I*) couples described in the first part of the Subsection.

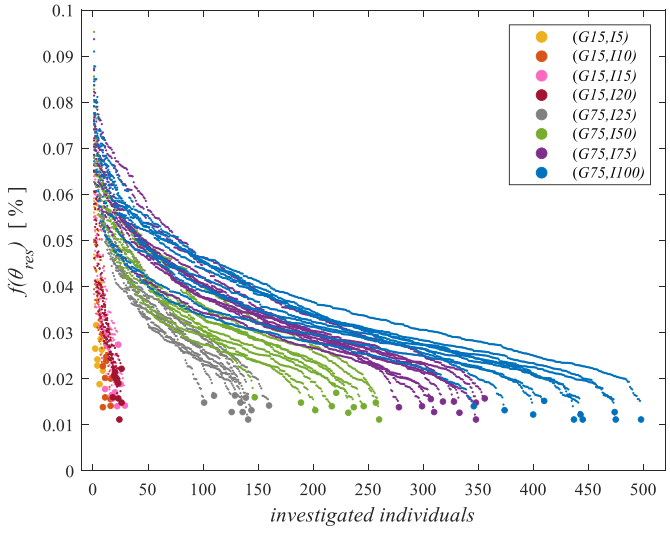

Fig. 9. Results of the sensitivity analysis for $G = 15$ and $I = 5$, 10, 15, 20, $G = 75$ and $I = 25$, 50, 75, 100. Values of the *Fitness-Function* $f(\theta_{res})$ for the investigated individuals.

In this regard, the analyses show that for each (*G, I*), the GA is able to find a *Most-Fit* individual with $f(\theta_{res})_{MF}$ between 0.01% and 0.04%, starting from a random initial individual. With respect to the *Less-Fit* individual with $f(\theta_{res})_{LF}$ equal to 0.095%, the GA leads to a reduction of $f(\theta_{res})$ between 60% and 90%.

In order to examine the computational demand of the GA, Fig. 10 (a)

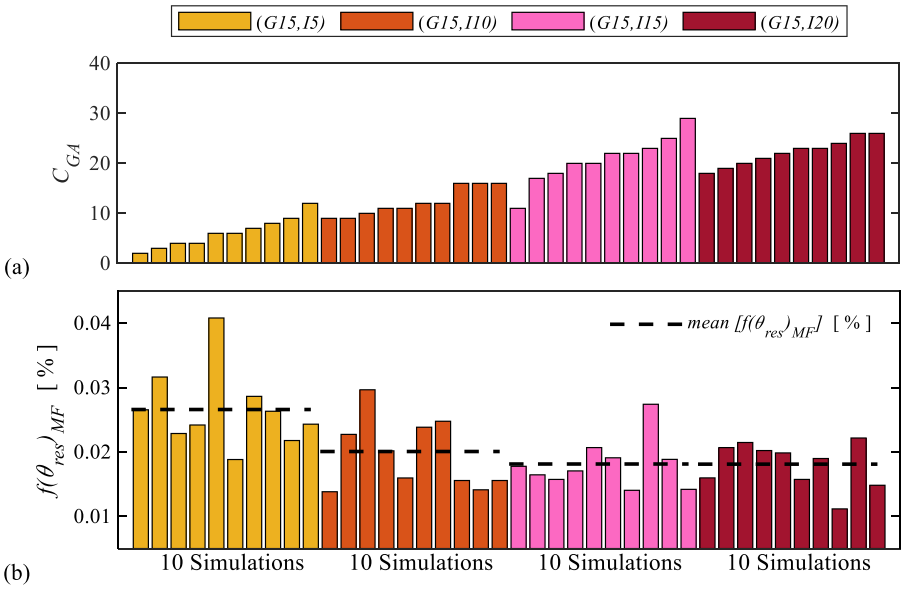

Fig. 10. Results of the sensitivity analysis for $G = 15$ and $I = 5$, 10, 15, 20. (a) Number of investigated individuals (C_{GA}). (b) *Fitness-Function* of the *Most-Fit* individuals ($f(\theta_{res})_{MF}$) and mean values of for each (G, I) ($mean[f(\theta_{res})_{MF}]$).

and Fig. 11 (a) show the ascending order of C_{GA} for each simulation with G equal to 15 and 75. Consequently, Fig. 10 (b) and Fig. 11 (b) show the corresponding values of $f(\theta_{res})_{MF}$ and their mean values for each (G, I) (*i.e.*, black dotted lines). As a reference, the *Fitness-Function* is also calculated for the two reference configurations (*i.e.*, MRF and M-BCJ), providing values of 0.174% and 0.0006% ~ 0, respectively, for the MRF and M-BCJ.

The results in Fig. 9, Fig. 10 (a), and Fig. 11 (a) show that increasing the number of G or I leads to higher C_{GA}, hence higher computational effort. Nevertheless, Fig. 9, Fig. 10 (b), and Fig. 11 (b) show that a higher C_{GA} leads to smaller values of $f(\theta_{res})_{MF}$ hence a higher chance of obtaining a *Most-Fit* individual who is closer to the *Best-Fit* individual (*i.e.*, $f(\theta_{res})_{MF} \sim f(\theta_{res})_{BF}$). For example, the mean values of $f(\theta_{res})_{MF}$ are 0.027%, 0.018%, and 0.014%, respectively with (*G15*, *I5*), (*G15*, *I15*), and (*G75*, *I25*). Additionally, it is possible to observe that for G equal to 15, increasing the values of I leads to smaller values of $f(\theta_{res})_{MF}$; conversely, for G equal to 75, the results obtained with I equal to 25, 50, 75, and 100 are very close. This is due to the fact that with (*G75*, *I25*), C_{GA} is already large enough to investigate a number of individuals such that the solution is reliable and effective. Therefore, increasing the values of I does not significantly affect the definition of the solution.

Fig. 12 (a) and (b) show the results of the thirty-two (G, I) investigated in the sensitivity analysis (Table 2). In Fig. 12 (a) and (b), each vertical stripe refers to a specific (G, I). In Fig. 12 (b), the black dots represent the values of $f(\theta_{res})_{MF}$ obtained in the 10 simulations, the red dash represents the mean value of $f(\theta_{res})_{MF}$ among the 10 simulations, and the grey bar shows the mean value of C_{GA} among the 10 simulations. Fig. 12 (a) shows the standard deviation of $f(\theta_{res})_{MF}$ among the 10 simulations.

The results obtained from the sensitivity analysis and presented in

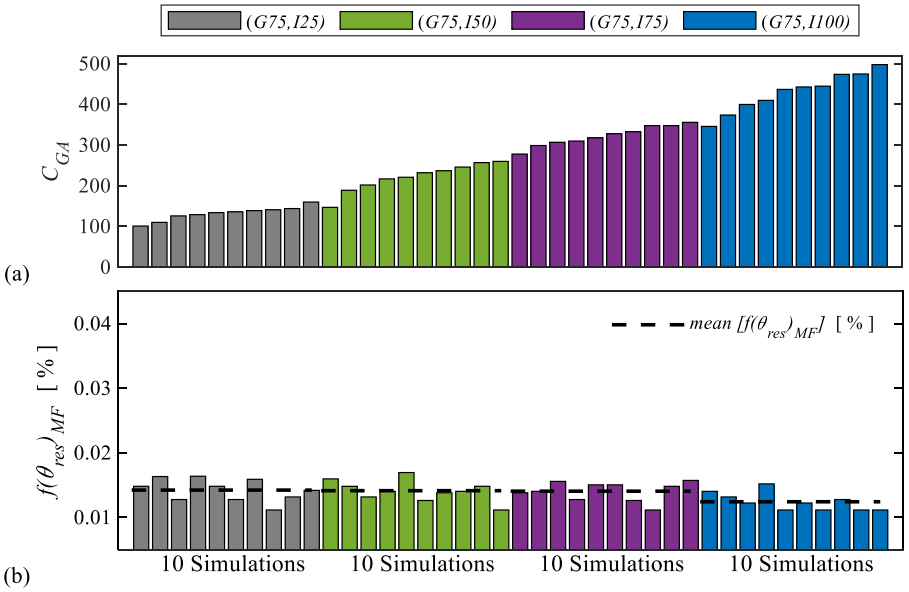

Fig. 11. Results of the sensitivity analysis for $G = 75$ and $I = 5$, 10, 15, 20. (a) Number of investigated individuals(C_{GA}). (b) *Fitness-Function* of the *Most-Fit* individuals ($f(\theta_{res})_{MF}$) and mean values for each (G, I) ($mean[f(\theta_{res})_{MF}]$).

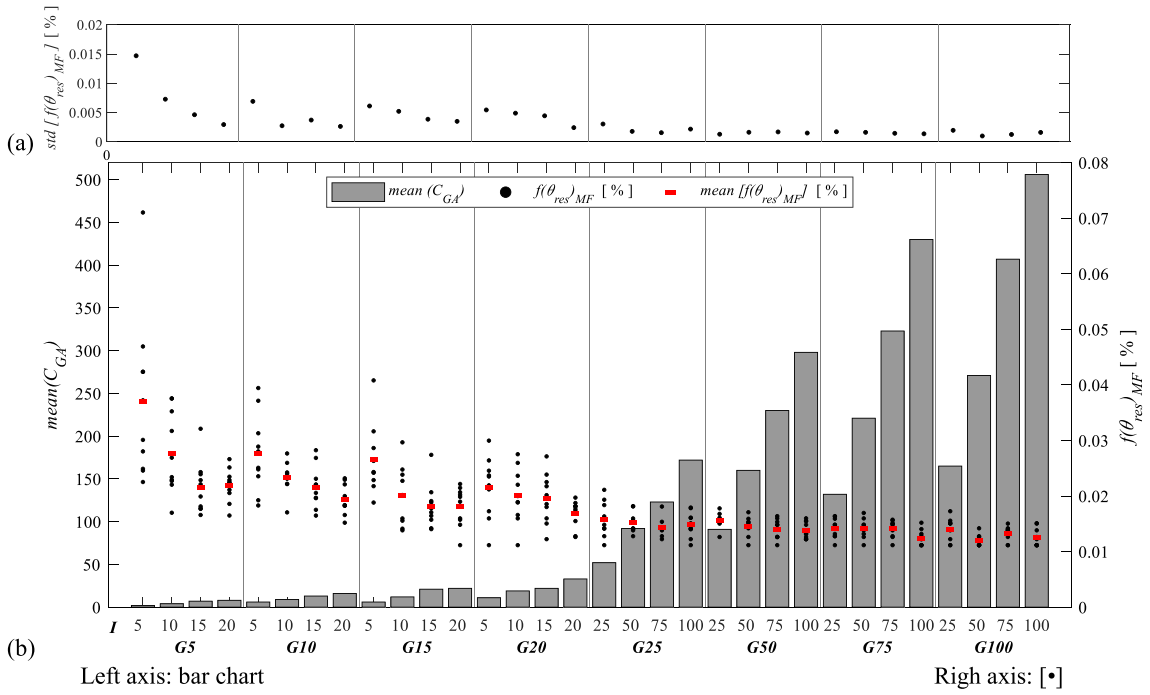

Fig. 12. Results of the sensitivity analysis for each (*G, I*). (b) Left axis - mean values of the number of investigated configurations (*mean*(C_{GA})). Right axis - *Fitness-Function* of the *Most-Fit* individuals ($f(\theta_{res})_{MF}$), mean values (*mean*[$f(\theta_{res})_{MF}$]) and (a) standard deviations (*std*[$f(\theta_{res})_{MF}$]) among the 10 simulations.

Fig. 12, show that increasing the values of the input parameters *G* and *I* leads to *i)* a less efficient solution with more computational effort (*i.e.,* higher numbers of investigated configurations (C_{GA})), *ii)* a more effective solution (*i.e., Most-Fit* individual closer to the *Best-Fit* individual), *iii)* more reliable solution with smaller values of uncertainties related to the randomness (*i.e.,* smaller values of *std*[$f(\theta_{res})_{MF}$]). Additionally, it is possible to observe for higher values of *G* and *I*, the values of the *mean*[$f(\theta_{res})_{MF}$] and *std*[$f(\theta_{res})_{MF}$] are asymptotically tending to $f(\theta_{res})_{BF}$ and 0, respectively. This means that, once this condition is reached, increasing the values of *G* and *I* has no advantages since it leads to a higher computational effort (C_{GA}) without any beneficial effects on the solution.

In conclusion, the values of *G* and *I* have to be chosen based on a compromise of: *i)* efficiency of the GA (*i.e.*, computational effort expressed in terms of number of investigated configurations), *ii)* reliability of the solution (*i.e.*, influence of the randomness on the GA's solution), *iii)* effectiveness of the solution (*i.e.*, how close is the *Most-Fit* solution to *Best-Fit* solution). The sensitivity analysis developed for this case study demonstrates that for the couple (*G25, I25*), the solution of the GA results in being stable, efficient, reliable, and effective.

4.4. Validation of the Genetic Algorithm (GA)

Validation of the GA is developed by solving the considered optimization problem with two different approaches: a *Brute-Force Approach* and the GA. The two approaches are applied to all the investigated scenarios (*i.e.*, S4, S8, S12, S16) with *Story-Restraint,* and the results are compared.

4.4.1. Brute-Force Approach

The *Brute-Force Approach* is used to investigate all the possible configurations with different placements of a given number of SCDF BCJs (n_{BCJ}) (referred to as individuals) and allows the definition of the best placement (referred to as *Best-Fit* individual).

The *Brute-Force Approach* is applied to all the investigated scenarios (*i.e.*, S4, S8, S12, S16) with *Story-Restraint*. Given a limited number of SCDF joints (n_{BCJ}) to be included in the MRF with *Story-Restraint*, the number of possible individuals ($C_{P.R}$), *i.e.*, configurations with different placements, can be calculated using the following equation (*i.e.,* the formula for the combinations of permutations without repetition:):

$$C_{P.R} = \frac{n!}{r!(n-r)!} \tag{6}$$

The number of possible configurations ($C_{P.R}$) for each scenario is reported in Table 3.

Fig. 13 shows the results of the *Brute-Force Approach* applied to S12 with *Story-Restraint*. According to Eq. (6), 56 possible individuals are defined and then evaluated through the *Fitness-Function*. Fig. 13 (a) shows the values of $f(\theta_{res})$ for the 56 possible individuals and some of the corresponding configurations. From here follows the configurations with all SCDF BCJs at specific stories are referred to as 'C' followed by the stories; for example, C134 is the configuration with all SCDF BCJs at stories 1, 3, and 4. The *Best-Fit* individual has $f(\theta_{res})_{BF}$ equal to 0.0298% and corresponds to C134. Conversely, the *Worst-Fit* individual has $f(\theta_{res})_{WF}$ equal to 0.15% and corresponds to C168. Fig. 13 (b) shows the configuration corresponding to the *Best-Fit* individual for S12.

Table 3 reports the results obtained from the *Brute-Force Approach* for each scenario with *Story-Restraint*, *i.e.*, the number of possible individuals ($C_{P.R}$), the configurations, and the values of the *Fitness-Function* ($f(\theta_{res})_{BF}$ and $f(\theta_{res})_{WF}$) corresponding to the *Best-* and *Worst-Fit* individuals. Moreover, to highlight the effect of the placement on the residual interstory drifts, Table 3 shows, for each scenario, $f(\theta_{res})$ reduction of the *Best-Fit* with respect to the *Worst-Fit* individual. These results demonstrate that both the number of SCDF BCJs and their placement have a significant effect on the residual interstory drifts.

Fig. 14 shows for scenarios S4, S8, S12, and S16 the configurations corresponding to the *Best-Fit* individuals.

4.4.2. Genetic Algorithm (GA)

The GA is applied to all the investigated scenarios (*i.e.*, S4, S8, S12, S16) with *Story-Restraint*. The number of generations (*G*) and individuals (*I*) are chosen according to the results of the sensitivity analysis of Subsection 4.3. In particular, *G* and *I* are assumed respectively equal to 75 and 25, which are identified as the upper-bound values for the GA.

Table 3
Results of the *Brute-Force Approach* with *Story-Restraint*.

S	n_{BCJ}	n	r	$C_{P.R}$	*Best-Fit*	$f(\theta_{res})_{BF}$ [%]	*Worst-Fit*	$f(\theta_{res})_{WF}$ [%]	$f(\theta_{res})$ reduction [%]
S4	4	8	1	8	C5	0.1069	C8	0.2032	47
S8	8	8	2	28	C34	0.0518	C78	0.1769	71
S12	12	8	3	56	C134	0.0298	C168	0.1512	80
S16	16	8	4	70	C1234	0.0154	C1578	0.0901	83

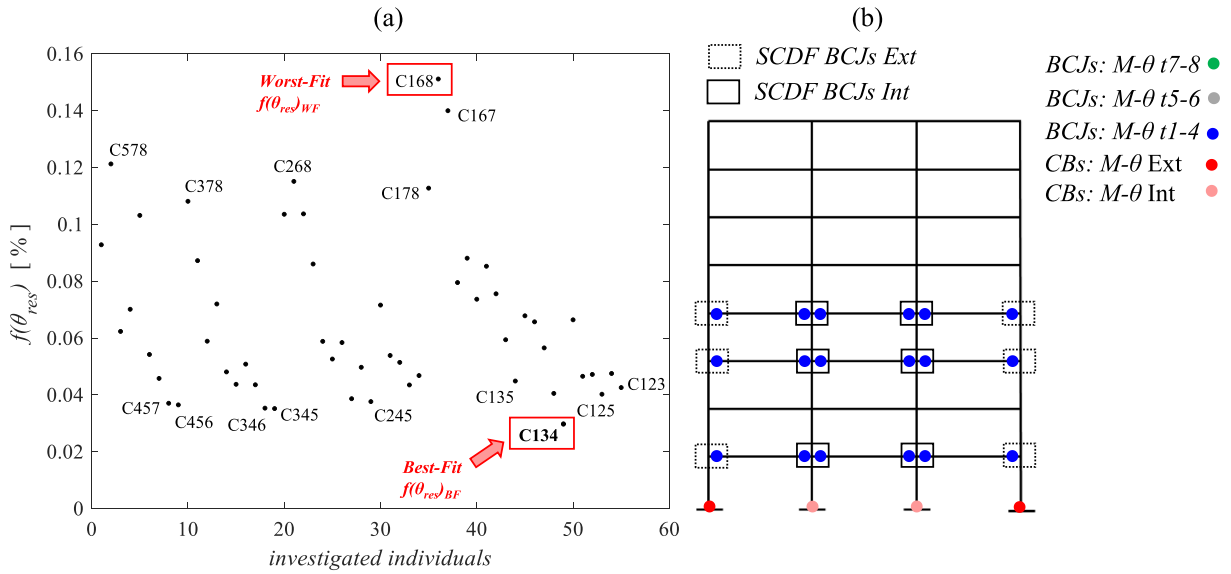

Fig. 13. Results of the *Brute-Force Approach* for scenario S12 with *Story-Restraint*. (a) Values of the *Fitness-Function* $f(\theta_{res})$ for all possible individuals ($C_{P.R}$). (b) Configuration corresponding to the *Best-Fit* individual.

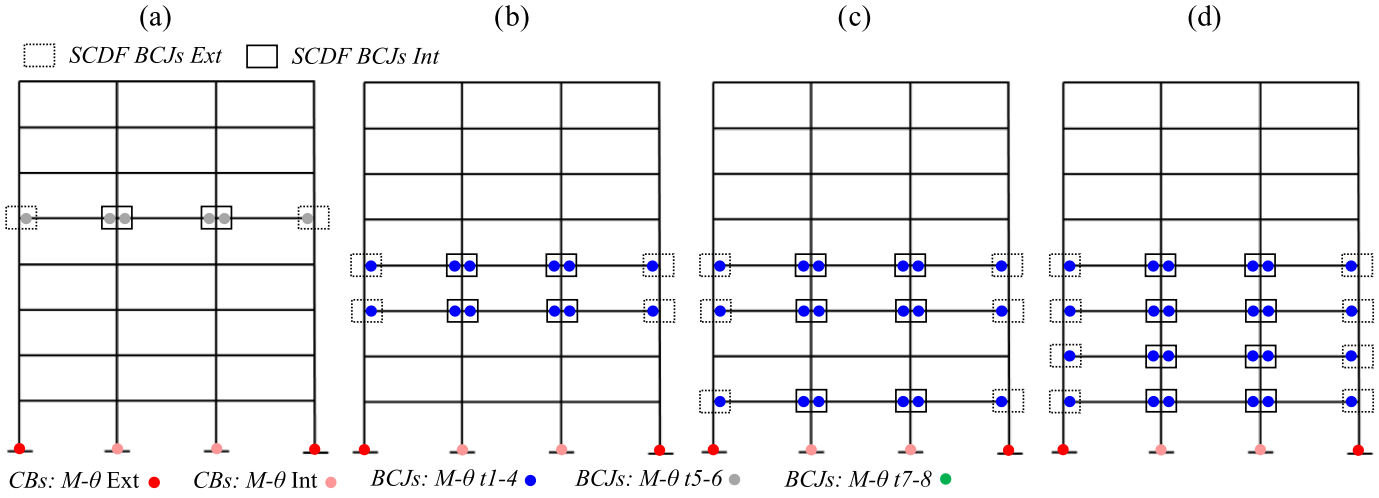

Fig. 14. Results of the *Brute-Force Approach* for scenarios with *Story-Restraint*. For each scenario representation of the configurations corresponding to the *Best-Fit* individuals. (a) S4, (b) S8, (c) S12 and (d) S16.

Fig. 15 shows the results of the GA applied to S12 with *Story-Restraint*. The GA investigates 36 (*i.e.*, C_{GA}) out of the 56 (*i.e.*, $C_{P.R}$) possible individuals. Fig. 15 (a) shows the values of the *Fitness-Function* ($f(\theta_{res})$) for the 36 investigated individuals. It is possible to observe that with respect to the *Less-Fit* individual with $f(\theta_{res})_{LF}$ equal to 0.15%, the GA finds a *Most-Fit* individual with $f(\theta_{res})_{MF}$ equal to 0.0298%, leading to a reduction of $f(\theta_{res})$ of about 80%. Fig. 15 (b) reports the vector of the *Most-Fit* individual, while Fig. 15 (c) shows the corresponding configuration.

Table 4 reports the results obtained from the GA for each scenario with *Story-Restraint, i.e.*, the number of investigated individuals (C_{GA}) which can be compared to the number of possible individuals ($C_{P.R}$) calculated according to Eq. (6), the configurations and the values of the *Fitness-Function* ($f(\theta_{res})_{MF}$ and $f(\theta_{res})_{LF}$) corresponding to the *Most-* and *Less-Fit* individuals.

4.4.3. Comparison of the results

The results obtained from the *Brute-Force Approach* (Subsection 4.4.1) and the GA (Subsection 4.4.2) are compared. For each scenario, both the approaches find the same solution for the optimization problem

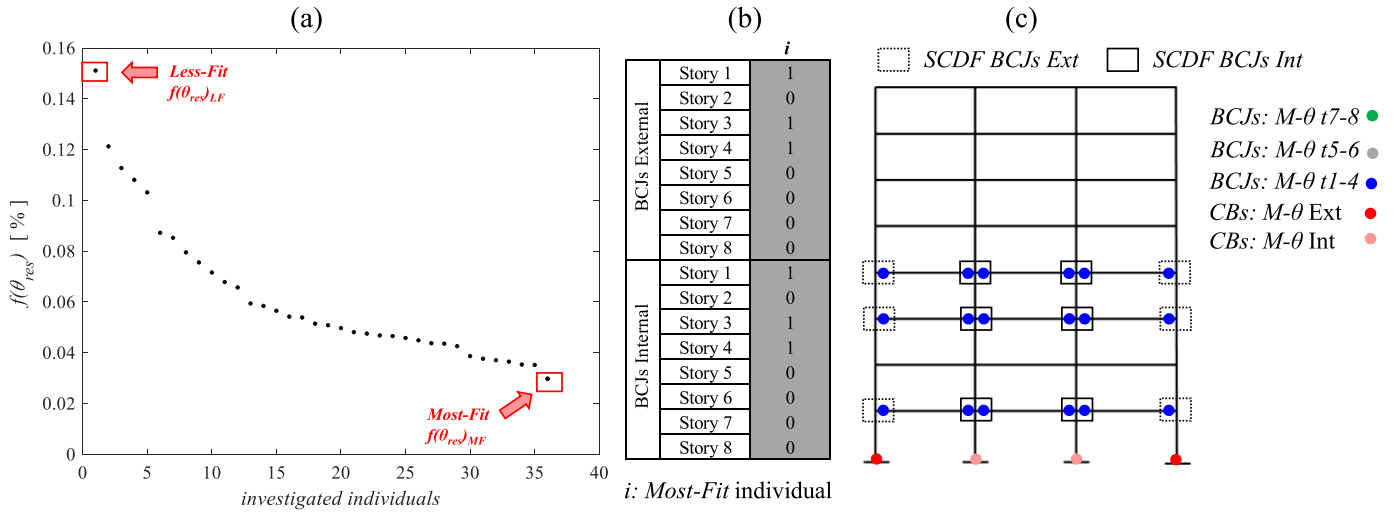

Fig. 15. Results of the GA for scenario S12 with *Story-Restraint*. (a) Values of the *Fitness-Function* $f(\theta_{res})$ for all the investigated individuals (C_{GA}). (b) Vector and (c) configuration corresponding to the *Most-Fit* individual.

Table 4
Results of the GA with *Story-Restraint*.

S	n_{BCJ}	$C_{P.R}$	$C_{GA.R}$	*Most-Fit*	$f(\theta_{res})_{MF}$ [%]	*Less-Fit*	$f(\theta_{res})_{LF}$ [%]
S4	4	8	6	C5	0.1069	C8	0.2032
S8	8	28	25	C34	0.0518	C68	0.1601
S12	12	56	36	C134	0.0298	C168	0.1512
S16	16	70	63	C1234	0.0154	C1368	0.0732

(*Best-Fit* and *Most-Fit* individuals are the same, respectively in Table 3 and Table 4). These results demonstrate the efficiency, reliability, and effectiveness of the GA and validate the proposed methodology. Additionally, it is observed that, while the *Brute-Force Approach* investigates all the possible configurations with different placement of the SCDF BCJs (C_P), the GA analyses a smaller number of configurations (C_{GA}), leading to a smaller computational effort. In scenario S4, the GA investigates 75% of the possible configurations (*i.e.*, 6 out of 8), in S8 the 89% (*i.e.*, 25 out of 28), in S12 the 64% (*i.e.*, 36 out of 56), in S16 the 90% (*i.e.*, 63 out of 70). It is worth mentioning that the advantage of the GA in finding the solution with less investigated configurations is more significant when the number of possible configurations is higher. This can be seen from the sensitivity analysis when the GA is applied to S16, with *no Story-Restraint* (Subsection 4.3). In this case, the possible configurations with different placements of SCDF BCJs are 4900 (C_P), and the GA investigates a different percentage of C_P based on the input values of *G* and *I* (Fig. 12). With (*G5*, *I5*) the GA investigates the 0.04% of the possible configurations (*i.e.*, 2 out of 4900), with (*G20*, *I15*) the 0.4% (*i.e.*, 22 out of 4900), with (*G50*, *I50*) the 3% (*i.e.*, 160 out of 4900), with (*G100*, *I100*) the 10% (*i.e.*, 160 out of 4900). This demonstrates the efficiency of the GA in finding a *Most-Fit* individual close to the *Best-Fit* individual, minimizing the computational effort.

5. Application of the Genetic Algorithm (GA)

The GA is applied to all the investigated scenarios (*i.e.*, S4, S8, S12, S16) with *no Story-Restraint*. The input parameters are chosen as described in Subsection 4.4.2 when the GA is applied with the *Story-Restraint*.

Fig. 16 shows the results of the GA applied to S4 with *no Story-Restraint*. The GA investigates 11 (*i.e.*, C_{GA}) out of the 64 (*i.e.*, $C_{P.R}$) possible individuals. Fig. 16 (a) shows the values of the *Fitness-Function* ($f(\theta_{res})$) for the 11 investigated individuals. Fig. 16 (b) and (c) show the vector and the configuration corresponding to the *Most-Fit* individual. Similarly, Fig. 17, Fig. 18, and Fig. 19 show the results for scenarios S8, S12, and S16.

Table 5 reports the results obtained from the GA for each scenario

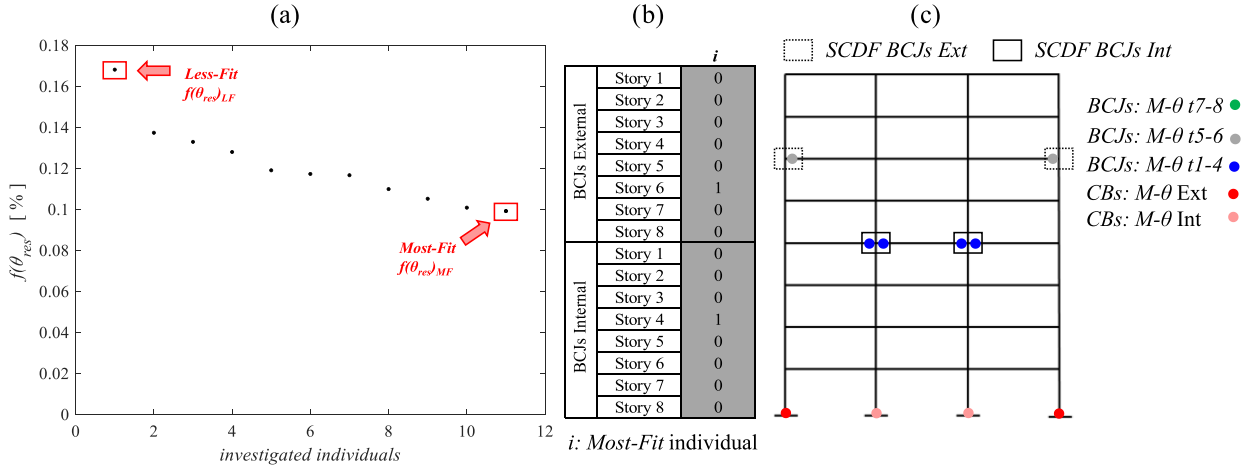

Fig. 16. Results of the GA for scenario S4 with *no Story-Restraint*. (a) Values of the *Fitness-Function* $f(\theta_{res})$ for all the investigated individuals (C_{GA}). (b) Vector and (c) configuration corresponding to the *Most-Fit* individual.

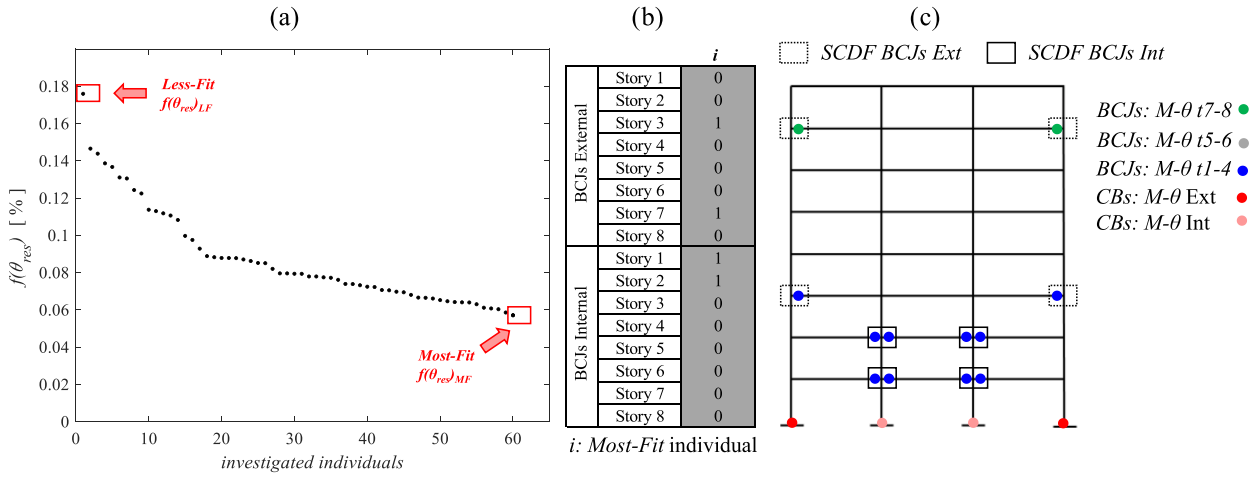

Fig. 17. Results of the GA for scenario S8 with *no Story-Restraint*. (a) Values of the *Fitness-Function* $f(\theta_{res})$ for all the investigated individuals (C_{GA}). (b) Vector and (c) configuration corresponding to the *Most-Fit* individual.

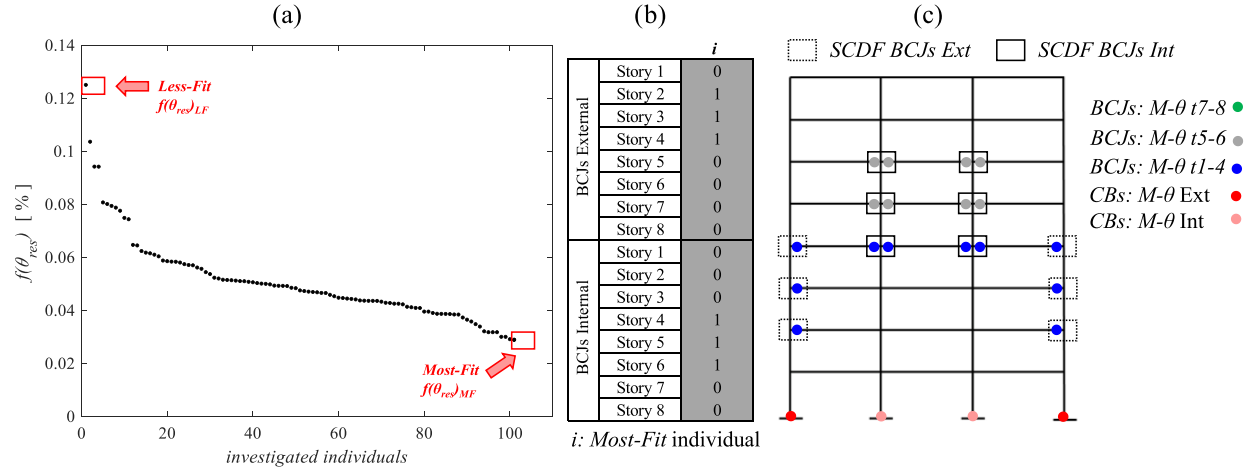

Fig. 18. Results of the GA for scenario S12 with *no Story-Restraint*. (a) Values of the *Fitness-Function* $f(\theta_{res})$ for all the investigated individuals (C_{GA}). (b) Vector and (c) configuration corresponding to the *Most-Fit* individual.

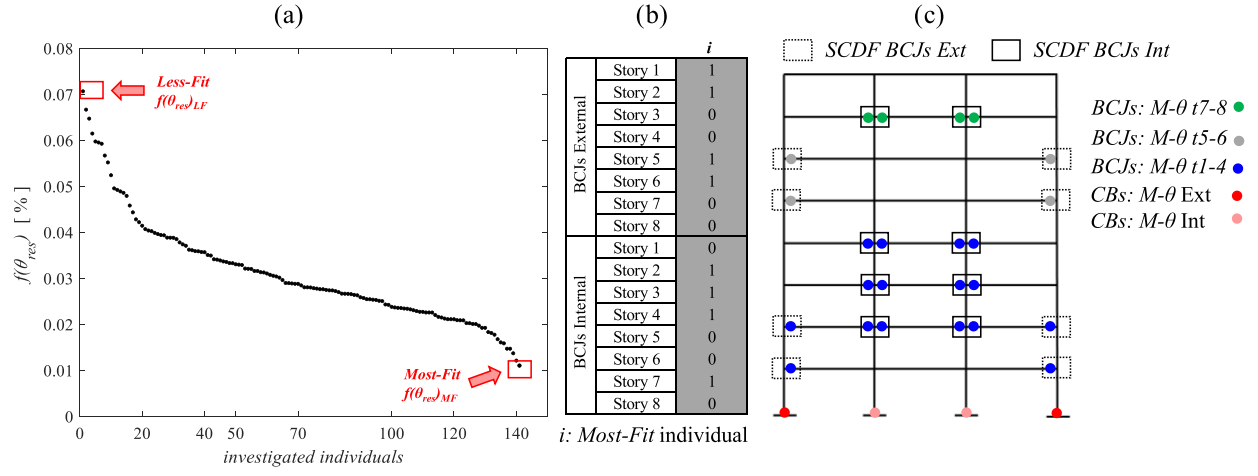

Fig. 19. Results of the GA for scenario S16 with *no Story-Restraint*. (a) Values of the *Fitness-Function* $f(\theta_{res})$ for all the investigated individuals (C_{GA}). (b) Vector and (c) configuration corresponding to the *Most-Fit* individual.

with *no Story-Restraint, i.e.*, the number of investigated individuals (C_{GA}) which can be compared to the number of possible individuals (C_P) calculated according to Eq.(5), the configurations and the values of the *Fitness-Function* ($f(\theta_{res})_{MF}$ and $f(\theta_{res})_{LF}$) corresponding to the *Most-* and *Less-Fit* individuals.

The *no Story-Restraint* assumption is equivalent to including an

Table 5
Results of the GA with *no Story-Restraint*.

S	n_{BCJ}	C_P	C_{GA}	*Most-Fit* SCDF BCJs at stories	$f(\theta_{res})_{MF}$ [%]	*Less-Fit* SCDF BCJs at stories	$f(\theta_{res})_{LF}$ [%]
S4	4	64	11	6-EXT; 4-INT	0.099	3-EXT; 8-INT	0.1682
S8	8	784	60	3,7-EXT; 1,2-INT	0.057	2,8-EXT; 7,8-INT	0.1760
S12	12	3136	101	2,3,4-EXT; 4,5,6-INT	0.029	3,6,7-EXT; 1,6,7-INT	0.1250
S16	16	4900	141	1,2,5,6-EXT; 2,3,4,7-INT	0.011	3,5,7,8-EXT; 2,6,7,8-INT	0.0708

additional variable and hence leads to a higher number of possible individuals. The results show that for each scenario, the values of $f(\theta_{res})$ with and with *no Story-Restraint* are very close and lead to a very similar reduction of $f(\theta_{res})$ with respect to the MRF. For example, for S4 the configuration with the optimal placement leads to a reduction of $f(\theta_{res})$ with respect to the MRF respectively of 37% and 42%, for S8 the percentage reductions are 70% and 66%, while 82% and 83%, and 91% and 93% are obtained for S12 and S16. Nevertheless, the number of investigated individuals with *no Story-Restraint* is significantly larger, leading to high computational demand. Therefore, using the *Story-Restraint* could result in a better strategy allowing the definition of optimal placements ensuring both easier design and lower structural complexity.

In order to provide the reader with a better understanding of the benefit and drawbacks of including a limited number of SCDF BCJs at specific locations, the following Section describes the deterministic response of scenario S12 under ground motion records considering both global and local Engineering Demand Parameters. Consistent results are obtained for all the other scenarios.

Fig. 20 shows a comparison between the conventional MRF and C134. Fig. 20 (a) shows the displacement time history with a single ground motion record for stories 3 and 4 which have all SCDF BCJs. Fig. 20 (b) and (c) show the height-wise distribution of the peak (θ_{peak}) and residual (θ_{res}) interstory drifts considering their median value among the seven ground motion records. The results highlight that including SCDF BCJs leads to higher peak interstory drifts, in particular on the stories where the SCDF BCJs are placed, but allows significantly reducing the residual interstory drifts with respect to the conventional structure [40].

Fig. 21 shows the comparison between the conventional MRF and the S12 configuration with the optimal placement obtained from the GA with *no Story-Restraint* (see Subsection 5). The damage status of both structures is monitored and compared to provide a qualitative interpretation of the problem from the mechanism analysis perspective. Fig. 21 (a) and (c) show the position of the plastic hinges respectively in the conventional MRF and the optimal configuration. Fig. 21 (b) shows the moment rotation behavior at specific locations. In the considered case study, it is assumed that the plastic hinges can form in specific critical locations (*i.e.*, at the beams' end and at the first story column's bases). In the conventional MRF (Fig. 21 (a)) 83% of the critical locations experience plastic deformations, while the remaining 17% have an elastic behavior. In the optimal configuration (Fig. 21 (c)) 42% of the critical locations are equipped with SCDF joints and show a flag-shape moment rotation behavior. The remaining critical locations have different behaviors depending on their position: 12% behave elastically and the remaining 46% have a hysteretic plastic behavior leading to the local damage of the structure. These results show that the optimal placement of a limited number of SCDF BCJs does not guarantee a full 'no damage' behavior but leads to a significant reduction of structural damage (*i.e.*, a lower number of plastic hinges) and significant benefits for the reparation (*i.e.,* small residual drifts).

6. Conclusions

The optimization problem considered in this study aims at defining the optimal placement of a given and limited number of Self-Centering Damage-Free (SCDF) Beam-to-Column Joints (BCJs) in steel Moment Resisting Frames (MRFs) such that their effectiveness in reducing residual drifts is maximized. The proposed methodology combines artificial intelligence techniques (*i.e.*, Genetic Algorithms) and seismic assessment methodologies (*i.e.*, non-linear time-history analyses) to solve the optimization problem. A Genetic Algorithm (GA) is implemented using a custom code written in Matlab, and non-linear time-history analyses are performed in OpenSees to calculate the *Fitness-Function*. A sensitivity analysis is performed on the GA to provide the user with a qualitative understanding of how to select the GA's input parameters such that a good compromise between computational effort and accuracy of the solution is guaranteed. A *Brute-Force Approach*, investigating all the possible configurations with different placements of the SCDF BCJs, is applied, and the results are used to validate the proposed GA. An 8-story 3-bays steel MRF is selected as a case study

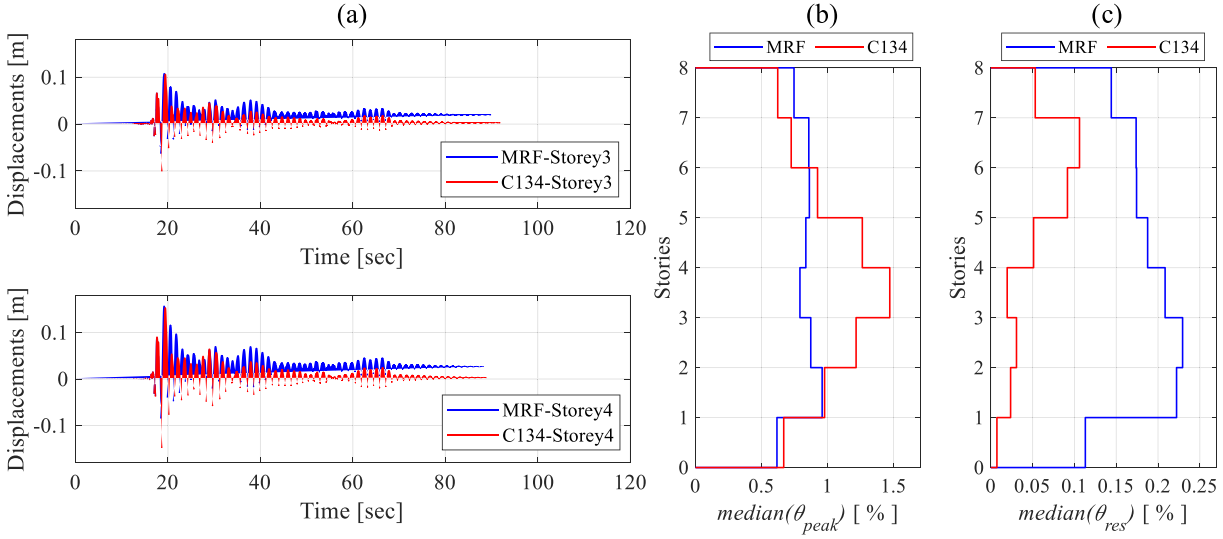

Fig. 20. Comparison between the dynamic response of the conventional MRF and C134. (a) Displacement time history with a single ground motion record for stories 3 and 4. (b) and (c): height-wise distribution of the peak (θ_{peak}) and residual (θ_{res}) interstory drifts (median value among the seven ground motion records).

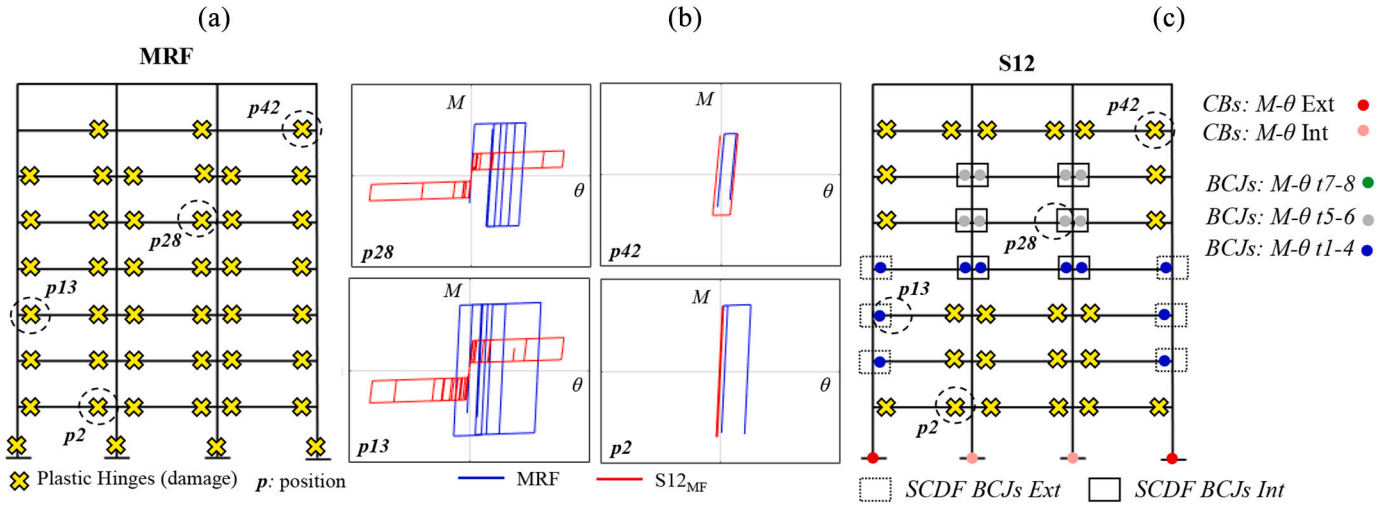

Fig. 21. Local behavior of the joints. Plastic hinges in the (a) conventional MRF and (c) optimal configuration of 12 SCDF BCJs with *no Story-Restraint.* (b) Moment-rotation behavior at specific positions with a single ground motion record.

structure, and a type of SCDF joint is taken into account. Two reference configurations are considered: the MRF with conventional CBs and full-strength BCJs, and the equivalent MRF with all SCDF CBs and BCJs. Moreover, four additional scenarios are defined based on the given number of SCDF BCJs to be included in the case study steel MRF. The conventional MRF is designed according to Eurocode 8 requirements, and the SCDF BCJs and CBs are designed following tailored design procedures already proposed and used in n previous studies by the Authors. Non-linear Finite Element Models are implemented in OpenSees and the GA is applied to the investigated scenarios. The following conclusions can be drawn:

- The proposed Genetic Algorithm represents an efficient procedure to define the optimal placement of a limited number of Self-Centering Damage-Free Beam-to-Column Joints in Self-Centering Steel Moment Resisting Frames.
- Although its intrinsic randomness, the Genetic Algorithm shows effectiveness, efficiency, and reliability in finding the solution to the optimization problem.
- The input parameters of the Genetic Algorithm can be chosen by the user as a compromise of reliability, effectiveness, and efficiency. The sensitivity analysis developed for the considered case study shows that considering a number of generations and new individuals larger than 25, the advantages in terms of reliability and effectiveness are negligible.
- The Genetic Algorithm finds the solution by investigating a limited percentage of the possible configurations requiring less computational effort than a *Brute-Force Approach.*
- Including a limited number of Self-Centering Damage-Free Beam-to-Column Joints is an effective strategy to ensure the self-centering capability of the structure hence controlling both the structural complexity and the construction cost.
- Given a number of SCDF BCJs to be included in the steel MRF employing their optimal placement leads to a significant improvement in terms of the self-centering capability with respect to a casual placement.
- Differentiating the properties of the Beam-to-Column Joints belonging to the same story may not be a convenient option with respect to the case where all Beam-to-Column Joints are characterized by the same properties (*i.e.,* all Self-Centering Damage-Free or all conventional). In fact, it leads to negligible improvements in terms of self-centering capability but significantly higher computational effort for the identification of the optimal placement.
- The results obtained in the present study refer to an earthquake intensity corresponding to the Ultimate Limit State in Eurocode 8 (*i.e.*, probability of exceedance of 10% in 50 years). The obtained results are coherent with a previous study from the Authors which demonstrated the efficiency and robustness of including a limited number of SCDF BCJs in steel MRFs for a wide range of intensities.

Declaration of Competing Interest

The authors declare that they have no known competing financial interests or personal relationships that could have appeared to influence the work reported in this paper.

Data availability

Data will be made available on request.

References

[1] N.F. Youssef, D. Bonowitz, J.L. Gross, A survey of steel moment-resisting frame buildings affected by the 1994 Northridge earthquake, Build. Fire Res. Lab. Natl. Inst. Stand. Technol. NISTIR 562 (1995) 173.
[2] D.K. Miller, Lessons learned from the Northridge earthquake, Eng. Struct. 20 (1998) 249–260, https://doi.org/10.1016/S0141-0296(97)00031-X.
[3] American Institute of Steel Construction: ANSI/AISC 341–16, Seismic Provisions for Structural Steel Buildings, 2016.
[4] European Committe for Standarization: EN 1998–1, Eurocode 8: Design of Structures for Earthquake Resistance – Part 1: General Rules, Seismic Actions and Rules for Buildings, 2004.
[5] F. Gutiérrez-Urzúa, F. Freddi, L. Di Sarno, Comparative analysis of code-based approaches for seismic assessment of existing steel moment resisting frames, J. Constr. Steel Res. 181 (2021), https://doi.org/10.1016/j.jcsr.2021.106589.
[6] F. Freddi, V. Novelli, R. Gentile, E. Veliu, S. Andreev, A. Andonov, F. Greco, E. Zhuleku, Observations from the 26th November 2019 Albania earthquake: the earthquake engineering field investigation team (EEFIT) mission, Bull. Earthq. Eng. 19 (2021) 2013–2044, https://doi.org/10.1007/s10518-021-01062-8.
[7] J. Mccormick, H. Aburano, M. Nakashima, Permissible residual deformation levels for building structures considering both safety and human elements, in: Proceedings of the 14th World Conference on Earthquake Engineering, 2008, pp. 12–17.
[8] C. Fang, W. Wang, C. Qiu, S. Hu, G.A. Macrae, M.R. Eatherton, Seismic resilient steel structures: A review of research, practice, challenges and opportunities, J. Constr. Steel Res. 191 (2022), https://doi.org/10.1016/j.jcsr.2022.107172.
[9] F. Freddi, C. Galasso, G. Cremen, A. Dall'Asta, L. Di Sarno, A. Giaralis, F. Gutiérrez-Urzúa, C. Málaga-Chuquitaype, S.A. Mitoulis, C. Petrone, A. Sextos, L. Sousa, K. Tarbali, E. Tubaldi, J. Wardman, G. Woo, Innovations in earthquake risk reduction for resilience: recent advances and challenges, Int. J. Disaster Risk Reduct. 60 (2021), 102267, https://doi.org/10.1016/j.ijdrr.2021.102267.
[10] S. Hu, W. Wang, B. Qu, Seismic economic losses in mid-rise steel buildings with conventional and emerging lateral force resisting systems, Eng. Struct. 204 (2020), 110021, https://doi.org/10.1016/j.engstruct.2019.110021.

[11] T.T. Soong, B.F. Spencer, Supplemental energy dissipation: state-of-the-art and state-of-the-practice, Eng. Struct. 24 (2002) 243–259, https://doi.org/10.1016/S0141-0296(01)00092-X.
[12] C.-Y. Seo, T.L. Karavasilis, J.M. Ricles, R. Sause, Seismic performance and probabilistic collapse resistance assessment of steel moment resisting frames with fluid viscous dampers, Earthq. Eng. Struct. Dyn. 43 (2014) 2135–2154, https://doi.org/10.1002/eqe.2440.
[13] F. Freddi, E. Tubaldi, A. Zona, Dall'Asta, A., Seismic performance of dual systems coupling moment-resisting and buckling-restrained braced frames, Earthq. Eng. Struct. Dyn. 50 (2021) 329–353, https://doi.org/10.1002/eqe.3332.
[14] F. Freddi, J. Ghosh, N. Kotoky, M. Raghunandan, Device uncertainty propagation in low-ductility RC frames retrofitted with BRBs for seismic risk mitigation, Earthq. Eng. Struct. Dyn. 50 (2021) 2488–2509, https://doi.org/10.1002/eqe.3456.
[15] L. Ragni, D. Cardone, N. Conte, A. Dall'Asta, A. Di Cesare, A. Flora, G. Leccese, F. Micozzi, C. Ponzo, Modelling and seismic response analysis of Italian code-conforming base-isolated buildings, J. Earthq. Eng. 22 (2018) 198–230, https://doi.org/10.1080/13632469.2018.1527263.
[16] S. Kitayama, M.C. Constantinou, Probabilistic seismic performance assessment of seismically isolated buildings designed by the procedures of ASCE/SEI 7 and other enhanced criteria, Eng. Struct. 179 (2019) 566–582, https://doi.org/10.1016/j.engstruct.2018.11.014.
[17] J.M. Kelly, Aseismic base isolation: review and bibliography, Soil Dyn. Earthq. Eng. 5 (1986) 202–216, https://doi.org/10.1016/0267-7261(86)90006-0.
[18] A. Martelli, P. Clemente, A. De Stefano, M. Forni, A. Salvatori, Recent development and application of seismic isolation and energy dissipation and conditions for their correct use, in: A. Ansal (Ed.), Perspectives on European Earthquake Engineering and Seismology vol. 1, Springer International Publishing, Cham, 2014, pp. 449–488.
[19] D. De Domenico, E. Tubaldi, I. Takewaki, T. Karavasilis, A. Dall'Asta, O. Lavan, Editorial: recent advances and applications of seismic isolation and energy dissipation devices, Front. Built Environ. 6 (2020), https://doi.org/10.3389/fbuil.2020.00126.
[20] M.R. Eatherton, L.A. Fahnestock, D.J. Miller, Computational study of self-centering buckling-restrained braced frame seismic performance, Earthq. Eng. Struct. Dyn. 43 (2014) 1897–1914, https://doi.org/10.1002/eqe.2428.
[21] J.M. Ricles, R. Sause, S.W. Peng, L.W. Lu, Experimental evaluation of earthquake resistant posttensioned steel connections, J. Struct. Eng. 128 (2002) 850–859, https://doi.org/10.1061/(ASCE)0733-9445(2002)128:7(850).
[22] H.-H. Khoo, C. Clifton, J. Butterworth, G. MacRae, Experimental study of full-scale self-centering sliding hinge joint connections with friction ring springs, J. Earthq. Eng. 17 (2013) 972–997, https://doi.org/10.1080/13632469.2013.787378.
[23] G.J. O'Reilly, J. Goggins, Experimental testing of a self-centring concentrically braced steel frame, Eng. Struct. 238 (2021), 111521, https://doi.org/10.1016/j.engstruct.2020.111521.
[24] S. Hu, W. Wang, B. Qu, Self-centering companion spines with friction spring dampers: validation test and direct displacement-based design, Eng. Struct. 238 (2021), 112191, https://doi.org/10.1016/j.engstruct.2021.112191.
[25] S. Hu, W. Wang, B. Qu, M.S. Alam, Development and validation test of a novel self-centering energy-absorbing dual rocking core (SEDRC) system for seismic resilience, Eng. Struct. 211 (2020), 110424, https://doi.org/10.1016/j.engstruct.2020.110424.
[26] S. Hu, W. Wang, B. Qu, M. Shahria Alam, Self-centering energy-absorbing rocking core system with friction spring damper: experiments, modeling and design, Eng. Struct. 225 (2020), 111338, https://doi.org/10.1016/j.engstruct.2020.111338.
[27] C. Qiu, X. Zhao, S. Zhu, Seismic upgrading of multistory steel moment-resisting frames by installing shape memory alloy braces: design method and performance evaluation, Struct. Control. Health Monit. 27 (2020), e2596, https://doi.org/10.1002/stc.2596.
[28] Y. Shen, F. Freddi, J. Li, Experimental and numerical investigations of the seismic behavior of socket and hybrid connections for PCFT bridge columns, Eng. Struct. 253 (2022), 113833, https://doi.org/10.1016/j.engstruct.2021.113833.
[29] C.A. Dimopoulos, F. Freddi, T.L. Karavasilis, G. Vasdravellis, Progressive collapse resistance of steel self-centering MRFs including the effects of the composite floor, Eng. Struct. 208 (2020), 109923, https://doi.org/10.1016/j.engstruct.2019.109923.
[30] M.M. Garlock, J.M. Ricles, R. Sause, Experimental studies of full-scale posttensioned steel connections, J. Struct. Eng. 131 (2004) 438–448, https://doi.org/10.1061/(ASCE)0733-9445(2005)131:3(438).
[31] G. Vasdravellis, T.L. Karavasilis, B. Uy, Large-scale experimental validation of steel posttensioned connections with web hourglass pins, J. Struct. Eng. 139 (2013) 1033–1042, https://doi.org/10.1061/(ASCE)ST.1943-541X.0000696.
[32] V.C. Kamperidis, T.L. Karavasilis, G. Vasdravellis, Self-centering steel column base with metallic energy dissipation devices, J. Constr. Steel Res. 149 (2018) 14–30, https://doi.org/10.1016/j.jcsr.2018.06.027.
[33] M. Latour, G. Rizzano, A. Santiago, L. Simões da Silva, Experimental response of a low-yielding, self-centering, rocking column base joint with friction dampers, Soil Dyn. Earthq. Eng. 116 (2019) 580–592, https://doi.org/10.1016/j.soildyn.2018.10.011.
[34] F. Freddi, C.A. Dimopoulos, T.L. Karavasilis, Experimental evaluation of a rocking damage-free steel column base with friction devices, J. Struct. Eng. 146 (2020) 4020217, https://doi.org/10.1061/(ASCE)ST.1943-541X.0002779.
[35] J.M. Ricles, R. Sause, M.M. Garlock, C. Zhao, Posttensioned seismic-resistant connections for steel frames, J. Struct. Eng. 127 (2001) 113–121, https://doi.org/10.1061/(ASCE)0733-9445(2001)127:2(113).
[36] H.J. Kim, C. Christopoulos, Seismic design procedure and seismic response of post-tensioned self-centering steel frames, Earthq. Eng. Struct. Dyn. 38 (2009) 355–376, https://doi.org/10.1002/eqe.859.
[37] F. Freddi, C.A. Dimopoulos, T.L. Karavasilis, Rocking damage-free steel column base with friction devices: design procedure and numerical evaluation, Earthq. Eng. Struct. Dyn. Struct. Dyn. 46 (2017) 2281–2300, https://doi.org/10.1002/eqe.2904.
[38] E. Elettore, F. Freddi, M. Latour, G. Rizzano, Design and analysis of a seismic resilient steel moment resisting frame equipped with damage-free self-centering column bases, J. Constr. Steel Res. 179 (2021), 106543, https://doi.org/10.1016/j.jcsr.2021.106543.
[39] E. Elettore, A. Lettieri, F. Freddi, M. Latour, G. Rizzano, Performance-based assessment of seismic-resilient steel moment resisting frames equipped with innovative column base connections, Structures. 32 (2021) 1646–1664, https://doi.org/10.1016/j.istruc.2021.03.072.
[40] L. Pieroni, F. Freddi, M. Latour, Effective placement of self-centering damage-free connections for seismic-resilient steel moment resisting frames, Earthq. Eng. Struct. Dyn. 51 (2022) 1292–1316, https://doi.org/10.1002/eqe.3615.
[41] R. Falcone, C. Lima, E. Martinelli, Soft computing techniques in structural and earthquake engineering: a literature review, Eng. Struct. 207 (2020), 110269, https://doi.org/10.1016/j.engstruct.2020.110269.
[42] G.M. Platt, X.S. Yang, A.J. Silva Neto, Computational Intelligence, Optimization and Inverse Problems with Applications in Engineering, 2018.
[43] J.H. Holland, C. Langton, S.W. Wilson, Complex Adaptive Systems Bradford Books Edition, 1992.
[44] D.E. Goldberg, M.P. Samtani, Engineering optimization via genetic algorithm, in: ASCE (Ed.), Proceedings pth Conference of Electronic Computation, 1986, pp. 471–482.
[45] S. Pezeshk, C.V. Camp, D. Chen, Design of nonlinear framed structures using genetic optimization, J. Struct. Eng. 126 (2000) 382–388, https://doi.org/10.1061/(ASCE)0733-9445(2000)126:3(382).
[46] M.-H. Ha, Q.-A. Vu, V.-H. Truong, Optimum design of stay cables of steel cable-stayed bridges using nonlinear inelastic analysis and genetic algorithm, Structures. 16 (2018) 288–302, https://doi.org/10.1016/j.istruc.2018.10.007.
[47] F. Di Trapani, A.P. Sberna, G.C. Marano, A new genetic algorithm-based framework for optimized design of steel-jacketing retrofitting in shear-critical and ductility-critical RC frame structures, Eng. Struct. 243 (2021), 112684, https://doi.org/10.1016/j.engstruct.2021.112684.
[48] G. Minafò, G. Camarda, Genetic Optimization for the design of seismic retrofitting of plane RC frames with Buckling Restrained Braces (BRBs), in: Conference: 8th International Conference on Computational Methods in Structural Dynamics and Earthquake Engineering COMPDYN 2021At: Athens (Greece), 2021, https://doi.org/10.7712/120121.8564.19069. Conference Proceeding ID: 19069.
[49] N. Wongprasert, M.D. Symans, Application of a genetic algorithm for optimal damper distribution within the nonlinear seismic benchmark building, J. Eng. Mech. 130 (2004) 401–406, https://doi.org/10.1061/(asce)0733-9399(2004)130:4(401).
[50] M.P. Singh, L.M. Moreschi, Optimal placement of dampers for passive response control, Earthq. Eng. Struct. Dyn. 31 (2002) 955–976, https://doi.org/10.1002/eqe.132.
[51] H. Movaffaghi, O. Friberg, Optimal placement of dampers in structures using genetic algorithm, Eng. Comput. (Swansea, Wales) 23 (2006) 597–606, https://doi.org/10.1108/02644400610680324.
[52] J.-R. Wu, L. Di Sarno, F. Freddi, M. D'Aniello, Modelling of masonry infills in existing steel moment-resisting frames: nonlinear force-displacement relationship, Eng. Struct. 267 (2023), https://doi.org/10.1016/j.engstruct.2022.114699.
[53] S. Mazzoni, F. McKenna, M.H. Scott, G.L. Fenves, OpenSEES: Open System for Earthquake Engineering Simulation, California, 2009.
[54] F.A. Charney, W.M. Downs, Modeling procedures for panel zone deformations in moment resisting frames, in: Connections in Steel Structures V. ESSC/AISC Workshop, 2004, pp. 121–130. Amsterdam.
[55] L.F. Ibarra, R.A. Medina, H. Krawinkler, Hysteretic models that incorporate strength and stiffness deterioration, Earthq. Eng. Struct. Dyn. 34 (2005) 1489, https://doi.org/10.1002/eqe.495.
[56] D.G. Lignos, H. Krawinkler, Deterioration modeling of steel components in support of collapse prediction of steel moment frames under earthquake loading, J. Struct. Eng. 137 (2011) 1291–1302, https://doi.org/10.1061/(asce)st.1943-541x.0000376.
[57] A. Lettieri, E. Elettore, L. Pieroni, F. Freddi, M. Latour, G. Rizzano, Parametric analysis of steel MRFs with self-centring column bases, Steel Constr. (2022), https://doi.org/10.1002/stco.202100050.
[58] I. Iervolino, C. Galasso, E. Cosenza, REXEL: computer aided record selection for code-based seismic structural analysis, Bull. Earthq. Eng. 82 (8) (2009) 339–362, https://doi.org/10.1007/S10518-009-9146-1.